Coherent interactions between optical photons using single atoms and atomic vapors.

Alexei Ourjoumtsev

Laboratoire Charles Fabry, Institut d'Optique, CNRS UMR 8501,
Université Paris-Sud

Mémoire d'Habilitation à Diriger les Recherches

COHERENT INTERACTIONS BETWEEN OPTICAL PHOTONS USING SINGLE ATOMS AND ATOMIC VAPORS.

Alexei Ourjoumtsev

Soutenue le 9 janvier 2015 devant la commission d'examen :

M.	Daniel	COMPARAT	Examinateur
M.	Daniel	ESTÈVE	Rapporteur
M.	Claude	FABRE	Rapporteur
M.	Philippe	GRANGIER	Examinateur
M.	Serge	HAROCHE	Président du jury
M.	Robin	KAISER	Rapporteur

À Matt. Merci pour tout.

Contents

1 Introduction **7**
- 1.1 Motivation . . . 7
- 1.2 State of the art . . . 8

2 Few-photon non-linearities induced by projective measurements **13**
- 2.1 Optical "Schrödinger's cats" . . . 13
- 2.2 Manipulating entanglement . . . 14
- 2.3 Perspectives . . . 15

3 Two-photon interactions in a strongly coupled atom-cavity system **17**
- 3.1 Theoretical background and experimental implementation . . . 17
- 3.2 Correlation spectroscopy of a two-photon resonance . . . 19
- 3.3 Emission of quadrature-squeezed light . . . 22
- 3.4 Feedback cooling of a single atom . . . 27
- 3.5 Outlook . . . 30

4 Interactions of optical photons in Rydberg atomic ensembles **32**
- 4.1 Introduction . . . 32
- 4.2 Experimental setup . . . 34
- 4.3 Non-linear dispersion of a Rydberg gas . . . 36
- 4.4 Homodyne tomography of a single photon retrieved from an atomic memory 41
- 4.5 Few-photon interactions in a Rydberg gas . . . 42

5 Outlook and conclusion **49**
- 5.1 On-going work . . . 49
- 5.2 Near-term projects . . . 50
- 5.3 General conclusion . . . 50

Chapter 1

Introduction

Contents

1.1 Motivation **7**
1.2 State of the art **8**
1.2.1 Hybrid systems 8
1.2.2 Projective measurements 8
1.2.3 Coupling to single quantum objects 9
1.2.4 Multi-level atomic ensembles 11

This manuscript summarizes my past and present research activities in quantum optics, with a particular focus on my post-doctoral work. In my ten-year-long career I explored three different approaches to address a fundamental problem: how to create strong coherent interactions between individual optical photons? In this introduction I will explain my interest in this question and list existing paths towards a possible answer. I will then present my contributions to this field since the my PhD thesis (briefly summarized in Chap 2), first as a post-doc in the Max Planck Institut für Quantenoptik (MPQ) in Garching (Chap. 3), then as a CNRS staff scientist in the Institut d'Optique in Palaiseau (Chap. 4). Finally, I will present my near-term directions and draw a general conclusion (Chap.5).

1.1 Motivation

First of all, contrary to the predictions of classical electrodynamics, light beams *may* spontaneously interact in vacuum. Classical Maxwell equations are indeed linear, but quantum electrodynamics allow photons to interact via transiently created virtual charged particle-antiparticle pairs. For photons in the visible range of the spectrum, however, the theoretical total scattering cross-section of this process is below 10^{-60} cm^2, and current experiments could only put an upper limit of $\sim 10^{-48}$ cm^2 to this value [1, 2]. Needless to say, light beams strongly interacting in vacuum have little chances to be seen outside science-fiction movies. Classical non-linear media are also of little help when the intensities of light beams are reduced to a single-photon level. For instance, observing a $\phi \sim \pi$ phase shift induced by one short single-photon pulse on another would require $\sim$ 10 000 km

of optical fiber [3], with a corresponding attenuation of 20 000 dB and a probability to recover both photons of 10^{-4000}... Conversely, keeping this probability to $\sim 50\%$ would limit the non-linear phase shift to $\phi \sim 10^{-6}$ in the most optimistic case. Creating a system one million times more efficient requires not only quantitative improvements but qualitative changes, and my interest in this problem mainly stems from the new physics it allows me to explore.

From a practical point of view, photon-photon interactions play a key role in quantum information processing (QIP). Although the most efficient systems to process quantum information locally are nowadays based on trapped ions or superconducting circuits, optical photons remain the only candidates to transmit this information between distant sites. Creating strong, coherent and lossless interactions between optical photons is a key requirement for developing quantum repeaters, a major current bottleneck for long-distance quantum communications. They are also necessary to deterministically create complex non-classical states of light for quantum computations or for precision measurements. In addition, recent theoretical proposals show that "quantum fluids" of interacting photons, combined with manipulation and detection tools available in quantum optics, could be used to simulate quantum effects occurring in condensed-matter systems [4].

1.2 State of the art

The problem of photonic interactions has mobilized the quantum optics community for decades and has been tackled by several methods.

1.2.1 Hybrid systems

From a purely pragmatic, QIP-oriented point of view, the weakness of photonic interactions can be circumvented by using photons only to transmit information, not to process it. This requires a linear interface to transfer qubits between photons and another QIP system where multi-qubit gates are easier to engineer, such as an ensemble of trapped ions or a superconducting microwave circuit [5, 6]. Since QIP-capable physical systems are nowadays quite diverse, the number of possible combinations is very large, opening many investigation paths and making this approach quite popular. However, transferring a quantum state from one system to another without errors is not an easy task. Realizing such light-matter interfaces is all the more challenging as the "matter" is not a passive homogeneous medium but a very complex system which must itself be manipulated at a single-excitation level.

1.2.2 Projective measurements

Another way to circumvent the problem is to allow photonic interactions to be probabilistic and use the fact that, besides unitary transformations, the evolution of a quantum system can be driven by projective measurements. Generally speaking, this approach consists in preparing an ensemble of entangled beams using standard tools such as parametric crystals and linear optics, and measuring some of these beams to project the others in a quantum state which depends on the measurement's outcome (Fig. 1.1). A specific outcome can then effectively "herald" a successful non-linear transformation.

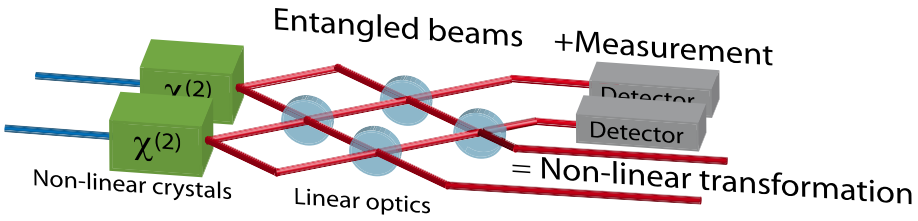

Figure 1.1: Typical structure of a setup to probabilistically create photonic interactions by projective measurements. Twin beams containing pairs of photons are produced by $\chi^{(2)}$ parametric crystals and combined using linear optics to create a specific entangled state. Some of the output beams are measured by photon counting or homodyne detection, projecting the others in a non-classical state depending on the measurement's outcome. For particular outcomes, this operation can mimic an effective interaction between these photons.

Historically, this method was the first to be actively developed, and it is still the most widespread for photonic quantum state manipulations. To date, this is the only approach which enabled true controlled quantum gates between optical photons [7]. Because a typical setup consists "only" of a laser, a few parametric crystals, linear optics and detectors, such experiments look simpler than those involving cold atoms or ions. However, they are very sensitive to imperfections: photons have many degrees of freedom, and it is quite challenging to control all of them at once. For instance, if a system is designed to process quantum states encoded on photonic polarization, it should preserve the spatial, spectral and temporal modes of the manipulated photons. Many experiments still leave this issue aside and simply post-select cases where all the expected photons are actually detected (regardless of their modal properties), discarding events where some of them are lost. Although this approach led to many proof-of principle demonstrations, such states can seldom be used as a QIP resource.

One my PhD thesis goals was to prepare quantum states pure enough to be used in QIP without post-selection. Another point was to develop new experimental methods combining two different "toolboxes" of quantum optics, one treating light as an ensemble of discrete photons, the other describing it in terms of continuous variables (quadratures). As this work has been presented in my PhD thesis [8] and in several publications, I will discuss it only briefly in Chap. 2, to put its results in perspective with other approaches.

Nowadays, the major challenge of this community is to manipulate larger quantum states without being hampered by the probabilistic nature of projective measurements. Because they usually require a tradeoff between the state's purity and its generation rate, these measurements succeed only rarely, and the probability to successfully perform several of them decreases exponentially with their number. A possible solution is to store successfully prepared states in a quantum memory until the preparation of others succeeds. Developing such quantum memories seems to be the next big step along this path towards scalable QIP.

1.2.3 Coupling to single quantum objects

Most generally, a quantum non-linear system must respond differently when excited with two photons rather than one. It is naturally the case for single quantum objects such as single atoms or ions, which present very anharmonic energy level spectra. By tuning the

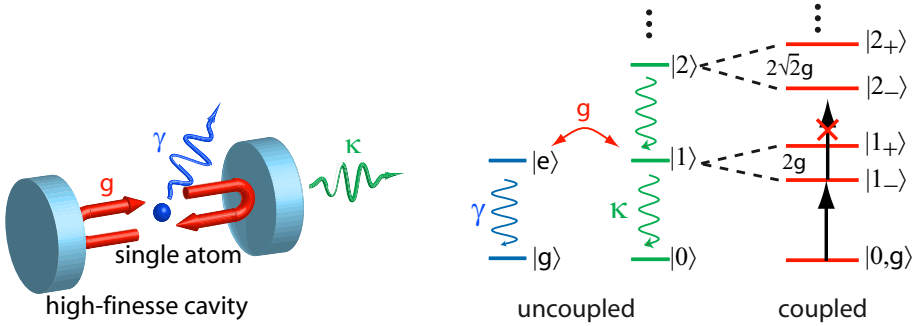

Figure 1.2: Example of a system leading to strong photon-photon interactions inside a high-finesse optical cavity mediated by a single quantum object, here a two-level atom. When the coupling rate $g = -\mathbf{d}.\mathbf{E}/\hbar$ between the atomic dipole $\mathbf{d}$ and the cavity electric field $\mathbf{E}$ exceeds their respective decay rates γ and κ, the energy spectrum of the system becomes anharmonic. The presence of one photon inside the cavity can then inhibit or enhance the transmission of another, depending on their frequencies. See Chap.3 for details.

light's frequency close to a transition between a ground state $|g\rangle$ and an excited state $|e\rangle$, one can treat these objects as two-level systems interacting with one photon at a time.

The scattering cross-section $\sigma \sim \lambda^2$ of resonant photon-atom interactions scales as the square of the transition's wavelength λ, with typical values around $\sigma \sim 10^{-9}$ cm^2 in the optical domain. Gigantic compared to the 10^{-60} cm^2 of free-space photon-photon scattering, this value nevertheless requires to focus light down to a sub-wavelength range. Free-space experiments along this line are now developed in Erlangen and Singapore [9, 10]. Most of the time, however, a sufficiently strong atom-light coupling is achieved with the assistance of high-finesse cavities. This "Cavity Quantum Electrodynamics" (CQED) approach was at the core of my post-doctoral work, and will be discussed in more detail in Chap.3. Its key prerequisite is to reach the so-called strong coupling regime where the atom and the cavity can exchange a photon several times before it is lost (Fig. 1.2). When the coupling is strong enough, the system becomes anharmonic and the presence of one photon modifies its response to another one. In addition, for practical applications photons must escape the cavity in a well-defined free-propagating mode rather than be randomly scattered in the environment.

This approach has been explored since the 1990's but systems satisfying both criteria above remain hard to come by. Among the best-known CQED experiments, those done in the group of Serge Haroche in Paris use microwave transitions between highly-excited Rydberg states [11]. They benefit from large atomic dipoles and slow decay rates as well as from the possibility to make extremely high-quality superconducting microwave cavities, but photons manipulated in these experiments remain trapped inside the resonator. In the optical domain, similar experiments were initiated in the group of Jeff Kimble at Caltech [12] and successfully developed by many other teams. Recent research efforts focus on high-quality integrable resonators, but compared to the microwave regime their optical and geometrical properties still restrict either the atom-cavity coupling or the photon extraction efficiency. Another major and general issue is to control the atomic motion in order to maintain a constant atom-cavity coupling.

Some of these problems can be solved by moving from "real" atoms to "artificial", solid-state ones. For microwave photons, this is done by the circuit-QED approach, combining

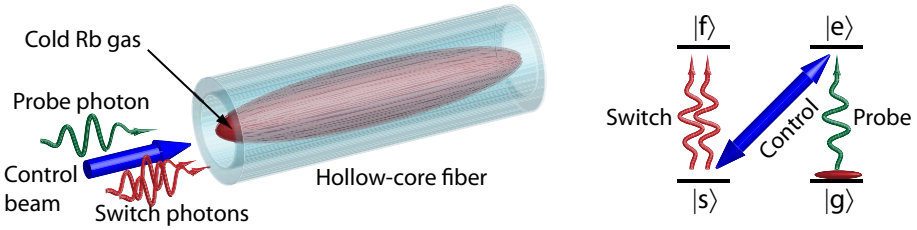

Figure 1.3: "Photonic switch" demonstrated by Bajcsy et al. [19] based on EIT in a cold Rb gas trapped inside a hollow-core optical fiber. In absence of switch photons, the control beam creates an EIT window allowing probe photons to be transmitted through the cloud, optically pumped in the state $|g\rangle$. Around 1000 switch photons per pulse are sufficient to disturb the EIT condition and make the cloud absorptive for probe photons.

microscopic superconducting LC resonators with non-linear elements based on Josephson junctions [13]. In the optical domain, it consists in embedding quantum dots inside semiconductor nanocavities [14, 15]. In both cases, one gets rid of detrimental effects due to atomic motion and benefits from very tight electric field confinements leading to large coupling constants. The impressive progress of these fields during the last few years [16, 17] makes it difficult to make firm statements about their limitations, but controlling complex inhomogeneous solid-state environments remains a challenge. It is particularly true in the optical domain, where fabrication processes are still partially random and do not allow one to reproducibly create identical devices.

1.2.4 Multi-level atomic ensembles

Given the difficulty to couple light to single quantum objects, an alternative consists in using collective coherent effects in multi-level optically dense atomic ensembles. In the simplest, Λ-type scheme, the manipulated photons are nearly resonant with the transition between a stable ground-state sublevel $|g\rangle$ and a short-lived excited state $|e\rangle$, while an auxiliary "control" laser beam couples $|e\rangle$ with another ground-state sublevel $|s\rangle$. The control beam creates a spectrally narrow electromagnetically-induced transparency (EIT) window, allowing photons to propagate through the gas as slow polarisation waves accumulating large non-linear phase shifts with little dissipation. Because this approach involves a spectrally narrow two-photon transition, it allows one to strongly decrease the photonic flux required to observe a non-linear effect. Unfortunately, this happens at the expense of a smaller bandwidth: despite the development of more sophisticated protocols [18] (Fig.1.3), the required number of photons per relevant temporal mode (defined by the inverse of the system's bandwidth) currently remains 3-4 orders of magnitude away from the single-photon regime [19].

Several theoretical proposals [20, 21] and a series of pioneering experiments in the group of Charles Adams in Durham [22] provided a new, original solution to this problem. In conventional EIT-based experiments, like in CQED, non-linearities arise from anharmonic level structures of individual atoms. The new approach, now actively studied in many groups, consists in using long-range interactions between *different* atoms instead. Such interactions can be created by modifying the EIT protocol: instead of a ground-state sublevel $|s\rangle$, the control beam couples the intermediate state $|e\rangle$ to an excited Rydberg level $|r\rangle$ with a principal quantum number $n \sim 100$. As such states have rather long

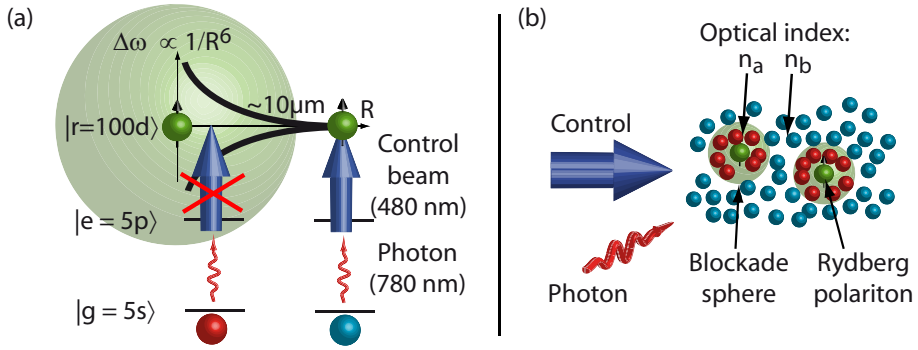

Figure 1.4: (a) Rydberg blockade mechanism. A Rydberg atom is excited via a two-photon transition involving a weak probe and a bright control beam. Due to strong van-der-Waals or dipole-dipole interactions, neighboring atoms located inside a "blockade sphere" are then shifted out of the two-photon resonance. (b) Optical non-linearity in a Rydberg-blockaded gas. In presence of the control beam near-infrared photons are converted to slowly propagating Rydberg polaritons. Each polariton creates a blockade sphere where the optical susceptibility of the gas is modified, leading to strong non-linear absorptive or dispersive effects. See Chap.4 for details.

lifetimes (a few $100\mu s$ in a room-temperature environment), this ladder-type three-level system responds like the "standard" Λ-type one to single photons, transmitted through the gas thanks to the EIT induced by the control beam. Two photons simultaneously injected in the gas, however, excite two Rydberg polarisation waves, which interact due to the very high polarisability of Rydberg states. This technique is used in my current experiments in Institut d'Optique, and will be discussed in detail in Chap.4. Although it is more recent than the others, it performs comparably well and makes fast progress. While other methods are mainly limited by practical issues, a major challenge here is to accurately model the many-body correlated quantum system used to create the desired non-linear effects. This difficulty, which may be seen as a hindrance for immediate practical applications, it from my point of view an interesting challenge in terms of fundamental physics and another reason to focus on this approach.

Chapter 2

Few-photon non-linearities induced by projective measurements

Contents

2.1 Optical "Schrödinger's cats" 13
2.2 Manipulating entanglement 14
2.3 Perspectives 15

This chapter will very briefly review my PhD thesis work, mainly to see what came out of it a few years later and to put it in perspective with my other projects.

2.1 Optical "Schrödinger's cats"

For publications related to this section, see Appendix **??,??,??** *or Refs. [23, 24, 25, 26, 27, 28]*

Referring to Schrödinger's paradox [29], a "Schrödinger's cat" can be defined as a system prepared in a quantum superposition of classical, macroscopically distinguishable states. Applied to quantum optics, this definition corresponds to a quantum superposition of "classical" coherent states:

$$|\psi_{cat}\rangle = \frac{|\alpha\rangle + \mathrm{e}^{i\phi}\,|-\alpha\rangle}{\sqrt{2\,(1+\cos(\phi)\mathrm{e}^{-2|\alpha|^2})}} \tag{2.1}$$

Besides their fundamental interest, these states are a useful resource for QIP and for precision measurements. In 2004-2005 we implemented the protocol proposed by Dakna et al. [30] to create "Schrödinger's kittens" with small coherent amplitudes $\alpha \approx 1$ by probabilistically subtracting a single photon from a squeezed vacuum beam [23]. This subtraction is done by reflecting a small fraction of a free-propagating squeezed vacuum pulse towards a photon counter, in a way that a photon detection heralds the subtraction of one (and most likely only one) photon from the beam. After improving the experimental setup developed by Jérôme Wenger during his PhD work [31], I managed to reconstruct the Wigner function of the produced "kittens' by homodyne tomography and observe

negative values as a signature of their non-classicality. Nowadays, these states became widely used as a resource for testing QIP protocols such as quantum teleportation [32]: their Wigner functions are phase-dependent and negative at the same time, which makes them a more insightful diagnostic tool than single photons, squeezed vacuum, or coherent states traditionally used in these protocols.

This first experiment had shown that one could apply discrete-variable tools (photon counting) to manipulate states typically described by their continuous variables, such as squeezed vacuum. In a later work, we demonstrated that the opposite was also true. We first generated and characterized photon number states $|n = 2\rangle$ containing 2 photons [24], then divided them on a 50/50 beamsplitter and measured one of the outputs with a homodyne detection: when the measurement's outcome was close to 0, this projected the other beam in a "cat" state larger than the "kittens" generated previously [25]. We demonstrated that by using photon-number states $|n\rangle$ containing n photons, this protocol allowed one to generate arbitrarily large cat states with $|\alpha|^2 \approx n$ in a more efficient way than other existing proposals.

2.2 Manipulating entanglement

For publications related to this section, see Appendix **??**,**??** *or Refs. [33, 34]*

A key result of my thesis work was to develop and demonstrate new, simple methods to protect fragile quantum states against losses.

The robustness of discrete-variable QIP, similarly to discrete-variable classical information processing, stems from the possibility to put a threshold on detected signals and discriminate between binary outcomes. In the quantum case, this threshold is usually the presence or the absence of a single photon, and many experiments post-select outcomes when a given number of photons was detected, neglecting those where some of the manipulated photons were lost. On the other hand, "continuous-variable" states, typically containing more than one photon per mode, are more complex and cannot be easily post-selected. This makes them very sensitive to optical losses and severely limits their applications in QIP.

My idea was to combine the best of both worlds and apply lossy operations to single photons only, leaving complex continuous-variable states unharmed. I used this approach to prepare Bell-like entangled cat states such as

$$|\psi\rangle = \frac{|\alpha\rangle\,|-\alpha\rangle - |-\alpha\rangle\,|\alpha\rangle}{\sqrt{2\,(1-\mathrm{e}^{-4|\alpha|^2})}}, \tag{2.2}$$

required for many QIP protocols. In principle, such states can be simply created by dividing a cat state $|\psi_{cat}\rangle \propto \left|\sqrt{2}\alpha\right\rangle - \left|-\sqrt{2}\alpha\right\rangle$ on a 50/50 beamsplitter. However, they are notoriously sensitive to losses, and transmitting the two resulting beams to distant partners through a lossy channel would completely destroy the state's non-classicality. We have shown that instead, one could locally create a cat state on each site and subtract a single photon delocalized between them to prepare the entangled state above [33]. Propagation losses are then only experienced by single photons and decrease the preparation success rate without significantly degrading the state's purity.

Like the subtraction of a single photon creating "Schrödinger's kittens", in this experiment the non-local photon subtraction was done by reflecting a small part of each of the manipulated modes 1 and 2 and making the reflected beams interfere before detecting a photon, thus implementing the superposition of two annihilation operators $(\hat{a}_1 + \hat{a}_2)/\sqrt{2}$. We have shown that this non-local photon subtraction could also be applied to quadrature-entangled EPR states to increase their entanglement [34]. This experiment allowed us to fully appreciate how important it was for projective measurements to be reliable. In some parameter regimes, where photon detection events were poorly correlated with an actual photon subtraction from the desired mode, this operation was completely counter-productive: the added randomness strongly degraded the final state's purity and decreased its entanglement instead of increasing it.

2.3 Perspectives

General methods presented above, combining discrete and continuous variables, evolved in an active sub-field of quantum optics, investigated by research groups in France, Germany, Italy, Danemark, Japan, USA, Canada... Like in our experiments, some of them use ultrafast pulsed lasers, which offer a relative experimental simplicity. In terms of state purity, however, continuous-wave (CW) experiments seem to hold the upper hand [35]. The possibility to control spectral and temporal aspects of manipulated states offers an extra degree of freedom [36] and, above all, the smaller bandwidth of states prepared with the CW approach is more compatible with existing quantum memories.

The main drawback of measurement-induced transformations is their probabilistic character. Intrinsically, current protocols have a tradeoff between the success rate p of a projective measurement and the fidelity ξ of the resulting state with the desired one. The best-known example is the preparation of single photons from parametric downconversion, where a brighter parametric source increases p but decreases ξ due to multi-photon contributions. The same issue occurs with photon subtraction, homodyne projective measurements, etc. In our experiments, $p \approx 1\%$ and $\xi \approx 80\%$ were typical values, which limited us to $2-3$ operations at most. With the substantial help of post-selection to simplify the preparation protocol, a recent experiment demonstrated eight-photon entangled states, with a preparation rate of ≈ 9 events per hour [37].

When trying to perform several transformations in parallel, a possible solution would be to store successfully prepared states in a memory and wait for other preparation steps to succeed. The overall success rate would then scale linearly rather than exponentially with the number of operations. Despite substantial progress during the past decade, experimentally demonstrated quantum memories still lack the ability to store a non-classical state, such as a photonic qubit or a "Schrödinger's kitten", for longer than it takes to generate another one. Storing and retrieving such states without losing their quantum features is, to my view, the next main challenge this community has to face.

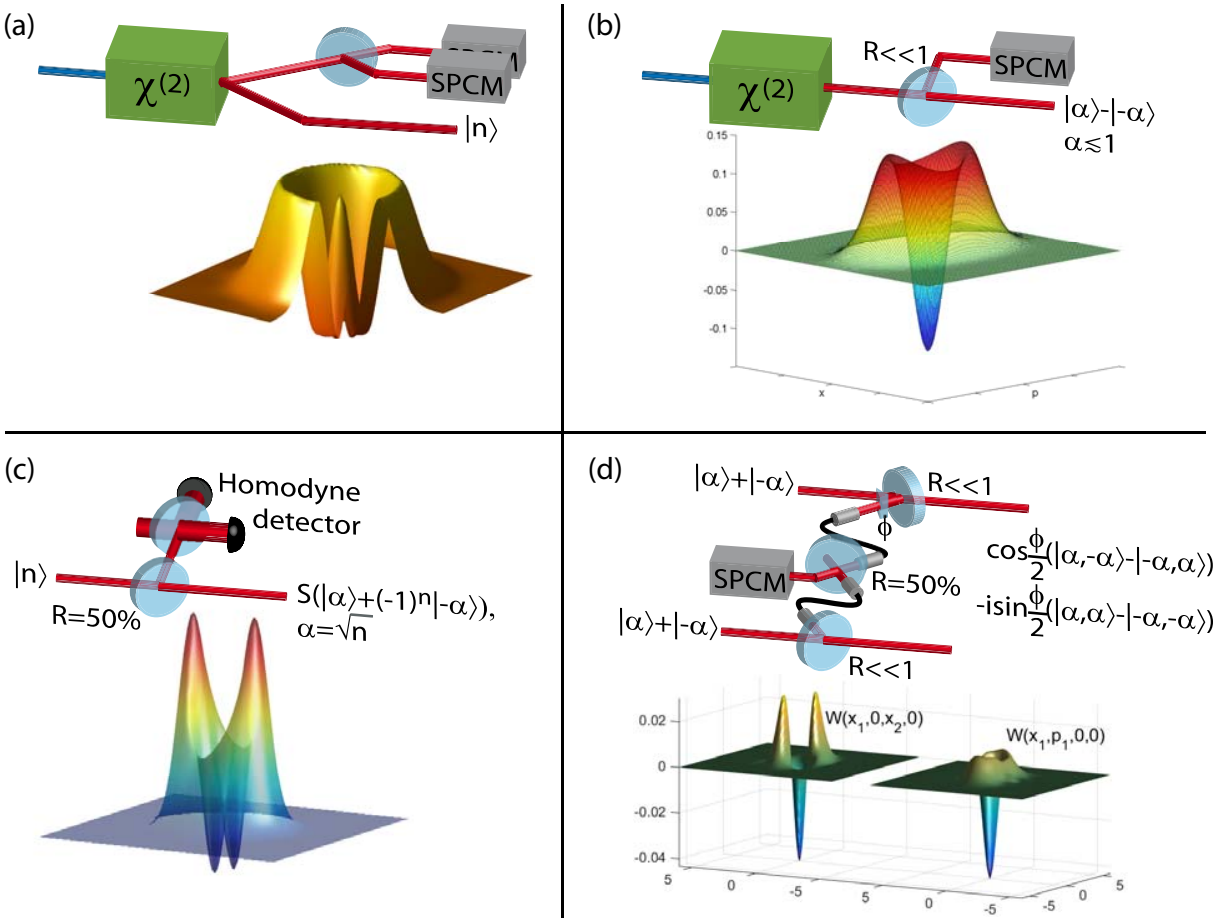

Figure 2.1: A few non-classical states prepared during my PhD thesis. (a) Top : a pair of "twin beams" is created using a non-degenerate optical parametric amplifier (OPA) based on a $\chi^{(2)}$ non-linear crystal. Detecting n photons in one of the beams (using n single photon counting modules, SPCMs) prepares a Fock state $|n\rangle$ in the other. Bottom: experimentally reconstructed Wigner function for $|n = 2\rangle$ [24]. (b) Top: A small fraction of a squeezed vacuum state, created by a degenerate OPA, is reflected towards a single photon counter which heralds the subtraction of a single photon. The resulting state resembles a "Schrödinger's kitten", a quantum superposition of coherent states $|\alpha\rangle$ and $|-\alpha\rangle$ with opposite phases and a small amplitude $\alpha \lesssim 1$. Bottom: experimentally measured Wigner function for $\alpha = 0.9$ [23]. (c) Top: Reflecting 50% of a Fock state $|n\rangle$ towards a homodyne detector ans measuring a quadrature value close to 0 prepares a squeezed "Schrödinger's cat" state with an amplitude $\alpha = \sqrt{n}$. Bottom: experimentally reconstructed Wigner function for an initial state $|n = 2\rangle$ [25]. (d) Top: Small fractions of two independent "cat" states propagate through lossy optical fibers and interfere on a 50/50 beamsplitter with a phase ϕ. Detecting a photon in one of the output ports creates an entangled superposition of coherent states shared between distant sites, in a way relatively immune to fiber losses. Bottom : "cuts" of experimentally measured two-mode Wigner functions for $\alpha = 0.8$ and $\phi = \pi/2$ [33].

Chapter 3

Two-photon interactions in a strongly coupled atom-cavity system

Contents

3.1 Theoretical background and experimental implementation 17
3.1.1 Strong coupling in cavity quantum electrodynamics (CQED) 17
3.1.2 Anharmonic response and few-photon non-linerities 18
3.1.3 Experimental setup 19
3.2 Correlation spectroscopy of a two-photon resonance 19
3.3 Emission of quadrature-squeezed light 22
3.4 Feedback cooling of a single atom 27
3.5 Outlook 30

3.1 Theoretical background and experimental implementation

3.1.1 Strong coupling in cavity quantum electrodynamics (CQED)

A single two-level atom coupled to a single mode of the electromagnetic field is one of the simplest quantum systems. Yet, after decades of theoretical and experimental investigations, the field of CQED is more active than ever [11]: alongside with ongoing experiments using bulk optical or microwave resonators, optical photons can now be strongly coupled to quantum dots inside semiconductor nanocavities, while microwave photons can be efficiently manipulated using superconducting circuits combining high-quality harmonic LC resonators with atom-like non-linear elements based on Josephson junctions. Of course, actual atoms (real or artificial) have more than two levels and actual cavities are seldom single-mode, but in a wide range of experimental situations the key physics of these systems is captured by the simple Jaynes-Cummings hamiltonian [38]

$$\hat{H}_0 = \omega_a \hat{a}^\dagger \hat{a} + \omega_c \hat{\sigma}^\dagger \hat{\sigma} + g(\hat{a}\hat{\sigma}^\dagger + \hat{a}^\dagger \hat{\sigma}), \tag{3.1}$$

where a cavity mode with a frequency ω_a, described by the annihilation operator $\hat{a}$, is nearly resonant with the transition between the ground state $|g\rangle$ and the excited state $|e\rangle$

of a single atom at a frequency ω_c, with $\hat{\sigma} = |g\rangle\langle e|$. The coupling between the atomic dipole $\mathbf{d}$ and the cavity electric field $\mathbf{E}$ then leads to the third term, governed by the coupling constant $g = -\mathbf{d}.\mathbf{E}/\hbar$.

The driven-dissipative nature of this system, essential to take into account, can be modeled by introducing the cavity field damping rate κ, the atomic dipole decay rate γ, and by assuming that the cavity mode is driven at a frequency ω by a coherent field with an amplitude α. In the rotating-wave approximation the system's density matrix $\hat{\rho}$ then follows the master equation

$$\begin{aligned}
\frac{\mathrm{d}\hat{\rho}}{\mathrm{d}t} &= -i[\hat{H},\hat{\rho}] + \mathcal{L}_a\hat{\rho} + \mathcal{L}_\sigma\hat{\rho}, && (3.2)\\
\hat{H}/\hbar &= -\delta_c\hat{a}^\dagger\hat{a} - \delta_a\hat{\sigma}^\dagger\hat{\sigma} + g(\hat{a}^\dagger\hat{\sigma} + \hat{a}\hat{\sigma}^\dagger) + \alpha(\hat{a} + \hat{a}^\dagger), && (3.3)\\
\delta_a &= \omega - \omega_a, && (3.4)\\
\delta_c &= \omega - \omega_c, && (3.5)\\
\mathcal{L}_a\hat{\rho} &= \kappa(2\hat{a}\hat{\rho}\hat{a}^\dagger - \hat{a}^\dagger\hat{a}\hat{\rho} - \hat{\rho}\hat{a}^\dagger\hat{a}), && (3.6)\\
\mathcal{L}_\sigma\hat{\rho} &= \gamma(2\hat{\sigma}\hat{\rho}\hat{\sigma}^\dagger - \hat{\sigma}^\dagger\hat{\sigma}\hat{\rho} - \hat{\rho}\hat{\sigma}^\dagger\hat{\sigma}). && (3.7)
\end{aligned}$$

When the single-atom cooperativity $C = g^2/2\kappa\gamma$ exceeds 1, the atom and the cavity form a strongly coupled system and can exchange a photon several times before it is lost. The system's spectrum is then formed of dressed states $|n\pm\rangle = a_\pm|g,n\rangle + b_\pm|e,n-1\rangle$ where n excitations are shared between the atom and the cavity. Using complex atom and cavity detunings $\Delta_a = \delta_a + i\gamma$ and $\Delta_c = \delta_c + i\kappa$, the complex detunings of these states can be expressed as

$$\Delta_{n\pm} = (n-1)\Delta_c + \frac{1}{2}(\Delta_c + \Delta_a) \mp \frac{1}{2}\sqrt{4ng^2 + (\Delta_c - \Delta_a)^2}. \quad (3.8)$$

Spectrally resolving the normal modes Δ_{1+} and Δ_{1-} is a characteristic feature of the strong coupling regime. For optical transitions, this has been achieved in the group of Jeff Kimble in 1992 using an atomic beam [39]. At the time when I started my post-doc in the group of Gerhard Rempe at the Max Planck Institute for Quantum Optics (MPQ) in 2007, optical frequency-resolved normal-mode resonances had been observed in a variety of experimental settings [40, 41, 42, 14, 15].

3.1.2 Anharmonic response and few-photon non-linerities

Reaching the strong coupling regime is necessary but insufficient to use these systems as strongly non-linear optical devices. In fact the normal-mode splitting is a classical effect, which would also occur for a completely linear system of two coupled harmonic oscillators. A few-photon non-linearity requires the system to respond differently to two excitations than to one, which means that one needs to spectrally resolve higher order states $|n,\pm\rangle$ with $n > 1$. This turns out to be a substantially more challenging task, as the spectral splitting between the n-photon transition to the state $|n,\pm\rangle$ and the $n+1$-photon transition to the state $|n+1,\pm\rangle$ decreases with n, as does the transition's strength. The cooperativity C must then be considerably larger than what is required to resolve the normal modes. Figure 3.1 illustrates this by showing two theoretical frequency-dependent transmission spectra of a coupled atom-cavity system. In case of a very strong coupling,

typical of what can be achieved in current microwave circuit QED experiments, the first few resonances are very well resolved. For values typical of our optical-domain experiment the splitting is much less pronounced, and one must detune the cavity from the atomic resonance in order to observe two-photon transitions to states $|2,\pm\rangle$ in the transmission spectrum. This experiment was done in our team immediately before I joined it [43]. The main part of my post-doctoral work consisted in further investigating these transitions in order to determine to what extent they could be used to create coherent interactions between free-propagating optical photons.

3.1.3 Experimental setup

Most of my work was done on a setup designed in the 1990's, which produced many interesting results before my arrival and which has been extensively described in a number of PhD thesis manuscripts [44, 45, 46, 47, 48]. By the time I joined the group it was an ageing machine, which motivated the construction of new, improved one [49]. Most of my post-doctoral work was done on the "old" setup before it was shut down and disassembled [50]. My contribution to experiments on the "new" setup was, to my view, rather limited.

Our experimental approach consisted in coupling single ^{85}Rb atoms to a $123\mu m$-long Fabry-Perot cavity with a finesse $\mathcal{F} \approx 450\,000$ (Fig.3.2) and an expected maximal atom-cavity coupling $g_{max}/2\pi = 16$ MHz exceeding the field decay rate $\kappa/2\pi = 1.3$ MHz and the dipole decay rate $\gamma/2\pi = 3$ MHz. Single atoms with nearly zero velocity were probabilistically injected in the cavity using an atomic fountain, and detected by a drop in the transmission of a weak probe beam at 780 nm driving a TEM_{00} cavity mode nearly resonant with the closed atomic transition $|g\rangle = \left|5S_{1/2}, F = 3, m_F = 3\right\rangle \rightarrow |e\rangle = \left|5P_{3/2}, F = 4,\, m_F = 4\right\rangle$. The atom was then captured by increasing the power of an intracavity red-detuned 785nm dipole trap beam. In some experiments, an additional blue-detuned "hollow" intracavity dipole trap was added. Once trapped, the atom experienced a sequence of alternating probing/cooling steps lasting a few 100 μs each. After 1 ms to 10 ms on average (depending on experimental settings), generally due to probe-induced heating, the atom escaped the trap and the sequence started over. By monitoring the probe's transmission during cooling intervals, we post-selected samples where the atom remained strongly coupled to the cavity: a transmission below 4% of its empty-cavity maximum ensured an average atom cavity coupling $g/2\pi = 12$ MHz.

3.2 Correlation spectroscopy of a two-photon resonance

For publications related to this section, see Appendix **??** *or Ref. [51]*

Spectrally addressing different coupled states $|n,\pm\rangle$ changes the quantum statistics of the transmitted photonic flux. Jeff Kimble's group demonstrated this in 2005 by driving a coupled atom-cavity system on the normal-mode resonance: as the beam was then off-resonant with multiply-excited states, the transmitted photons were antibunched [52]. We transposed this experiment to measure photon statistics on the two-photon resonance, where we expected an enhanced transmission of photon pairs.

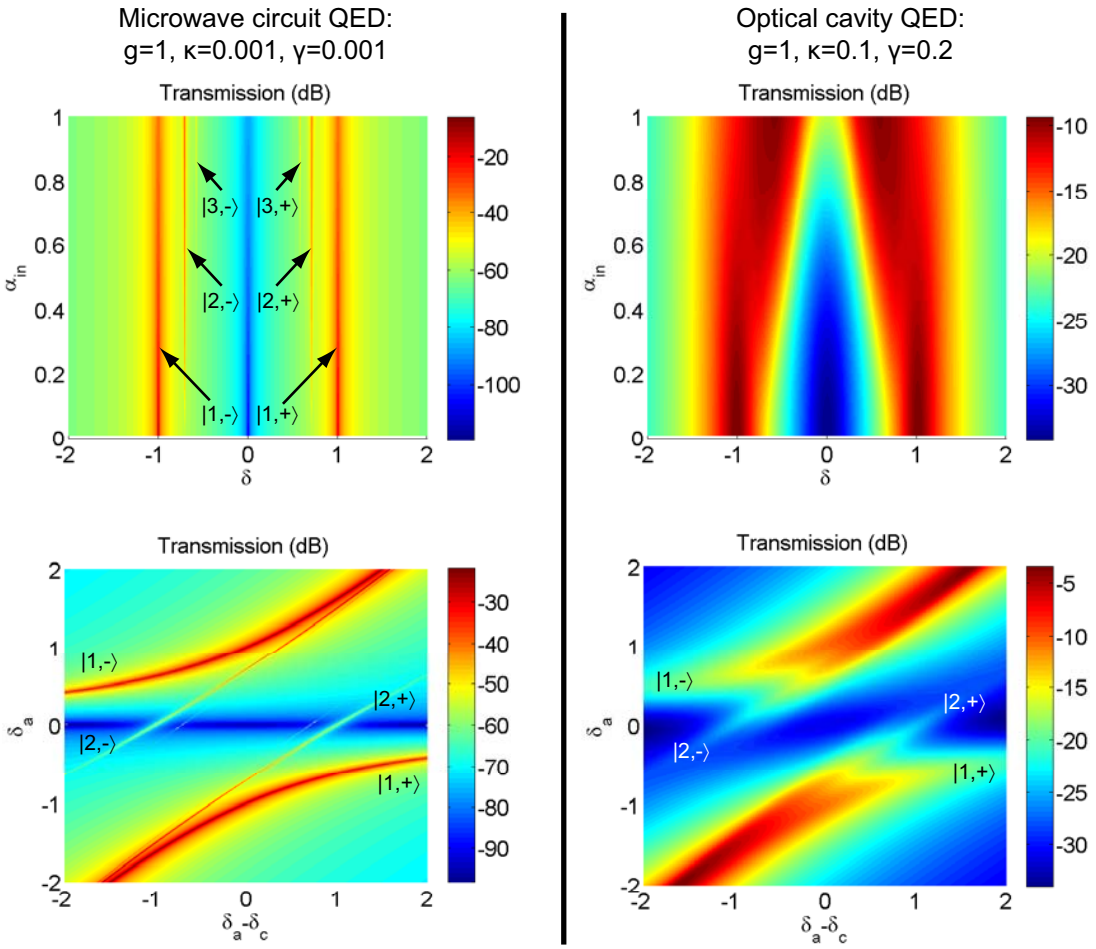

Figure 3.1: Transmission through a harmonic resonator coupled to a two-level "atom", calculated using Eq.3.2 with parameters typical for current experiments in microwave circuit QED (left) and in optical cavity QED (right). Upper row: transmission spectrum as a function of the impinging field amplitude α_{in} and the detuning $\delta = \delta_a = \delta_c$ (cavity resonant with the atom). The very strong coupling obtained in circuit QED allows one to clearly resolve multi-photon resonances appearing for $|\delta| < 1$. The coupling in optical cavity QED is too weak to resolve them in this case. Lower row: transmission spectrum as a function of the cavity-atom detuning $\delta_a - \delta_c = \omega_c - \omega_a$ and of the probe-cavity detuning δ_c, for $\alpha_{in} = 0.4$. Multi-photon resonances can clearly be seen between the two normal modes $|1, \pm\rangle$ in the circuit QED case. For the optical cavity QED regime, two-photon resonances can be resolved for $\delta_a \approx 0$ and $|\delta_a - \delta_c| \approx 1$.

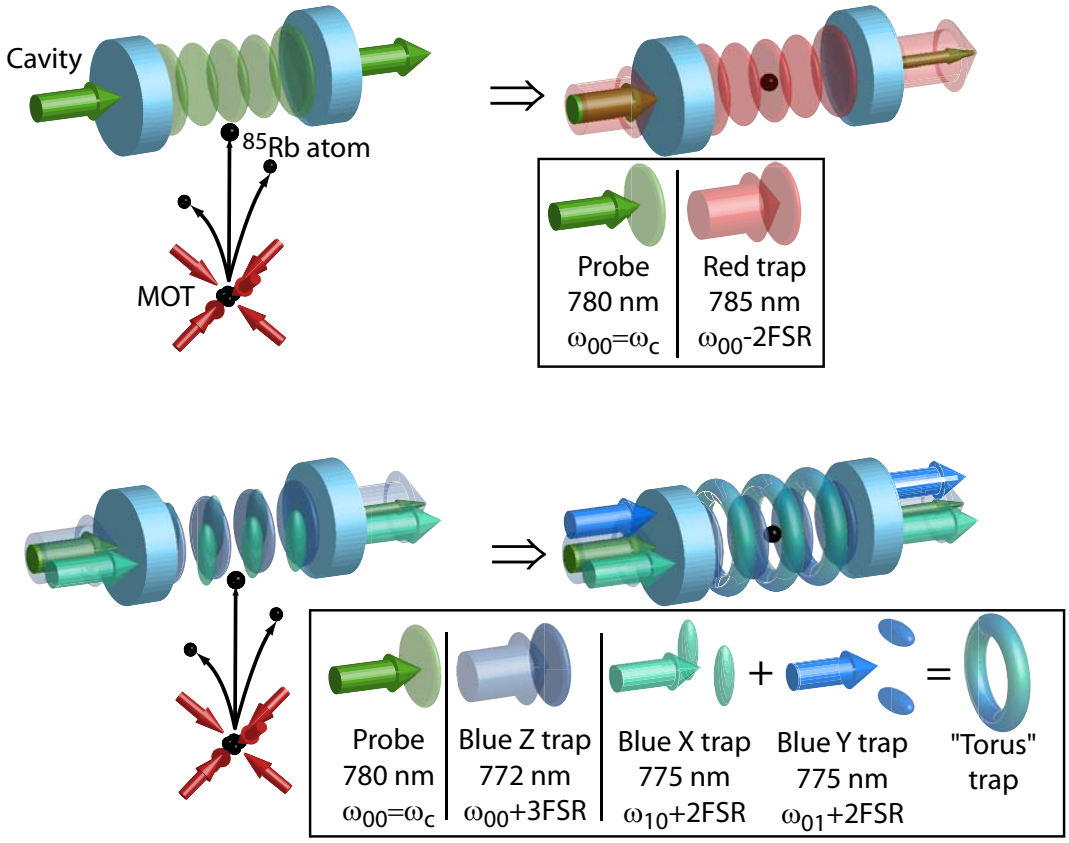

Figure 3.2: Trapping a single atom in a high-finesse Fabry-Perot cavity. (Top) A single atom is injected into the cavity using an atomic fountain. Its coupling to the TEM_{00} mode of the probe beam (frequency $\omega_{00} = \omega_c$) decreases the transmission of the latter. The atom is then captured in an attractive red-detuned dipole trap. (Bottom) Atomic capture using a blue-detuned trap. During the atomic injection, the standing-waves formed by the Z and X repulsive traps guide the atom towards an anti-node of the probe mode (not shown for clarity). A sufficiently strongly coupled atom, detected by a drop in the probe's transmission, is then captured by switching on the repulsive Y trap, which closes the trapping "light box" surrounding the atom.

The most commonly used figure of merit for two-photon correlations is the function

$$g^{(2)}(\tau) = \frac{\langle \hat{a}^\dagger(t)\hat{a}^\dagger(t+\tau)\hat{a}(t+\tau)\hat{a}(t)\rangle}{\langle \hat{a}^\dagger\hat{a}\rangle^2}, \tag{3.9}$$

independent on t in the steady-state regime and equal to 1 for a coherent state transmitted through the cavity in absence of non-linearity. While the minimum of $g^{(2)}(0)$ as a function of the probe frequency can indeed accurately locate a single-photon resonance, where the numerator $\langle(\hat{a}^\dagger)^2\hat{a}^2\rangle$ should ideally vanish, it does not necessarily show a maximum on two-photon resonances: although the numerator is maximal in this case, in the weak driving limit the denominator $\langle \hat{a}^\dagger\hat{a}\rangle^2$ mainly depends on single-photon physics and can present a minimum elsewhere. To circumvent this issue, we use the correlation function

$$C^{(2)}(\tau) = \langle \hat{a}^\dagger(t)\hat{a}^\dagger(t+\tau)\hat{a}(t+\tau)\hat{a}(t)\rangle - \langle \hat{a}^\dagger\hat{a}\rangle \tag{3.10}$$

which correctly locates the two-photon resonance, where $\langle(\hat{a}^\dagger)^2\hat{a}^2\rangle \gg \langle \hat{a}^\dagger\hat{a}\rangle^2$. The $C^{(2)}$ function is equal to zero for a linear coherently driven system, becomes negative on the single-photon resonances and positive on the two-photon resonances of the coupled atom-cavity system.

We measured this function using the Hanbury-Brown and Twiss (HBT) measurement scheme sketched on Fig. 3.3, by equally splitting the beam transmitted through the cavity between two single-photon counting modules. In order to spectrally resolve the two-photon resonance with the state $|2,-\rangle$ from the normal modes $|1,\pm\rangle$, following Fig.3.1 we used an atom-cavity detuning $|\delta_{ac}| \sim g$.

On the cavity resonance ($\delta_c = 0$), small oscillations of the atom in the trap strongly change the transmission, which creates spurious classical correlations dominating the measured $C^{(2)}(\tau)$. This effect disappears for $|\delta_c| > \gamma$. A narrow zero-delay correlation peak appears on the two-photon resonance, with a temporal width compatible with the system's quantum dynamics. This was confirmed by a measurement of the $g^{(2)}$ fonction on the two-photon resonance performed later with similar experimental parameters and an improved detection efficiency, which revealed damped oscillations in the time domain: upon detection of a first photon in a pair, the system performs vacuum Rabi oscillations between states $|g,1\rangle$ and $|e,0\rangle$ and decays to the ground state $|g,0\rangle$ [48]. The zero-delay function $C^{(2)}(0)$ measured for different detunings δ_c peaks on the two-photon resonance with the state $|2,-\rangle$, where the photon coincidence rate is enhanced by a factor ≈ 40 compared to a coherent state with the same intensity. Experimental data is consistently described by numerical simulations based on the master-equation model and including effects of atomic motion.

3.3 Emission of quadrature-squeezed light

For publications related to this section, see Appendix **??** *or Ref. [50]*

Previous experiments brought a new series of questions regarding the light emitted from the coupled atom-cavity system:

- What is its emission spectrum? As shown on Fig.3.4, a system excited with two photons at a frequency ω is expected to decay via one of the two normal modes $|1,-\rangle$ or $|1,+\rangle$, emitting photons frequency-shifted by $\pm\delta_{1,-}$ or $\pm\delta_{1,+}$.

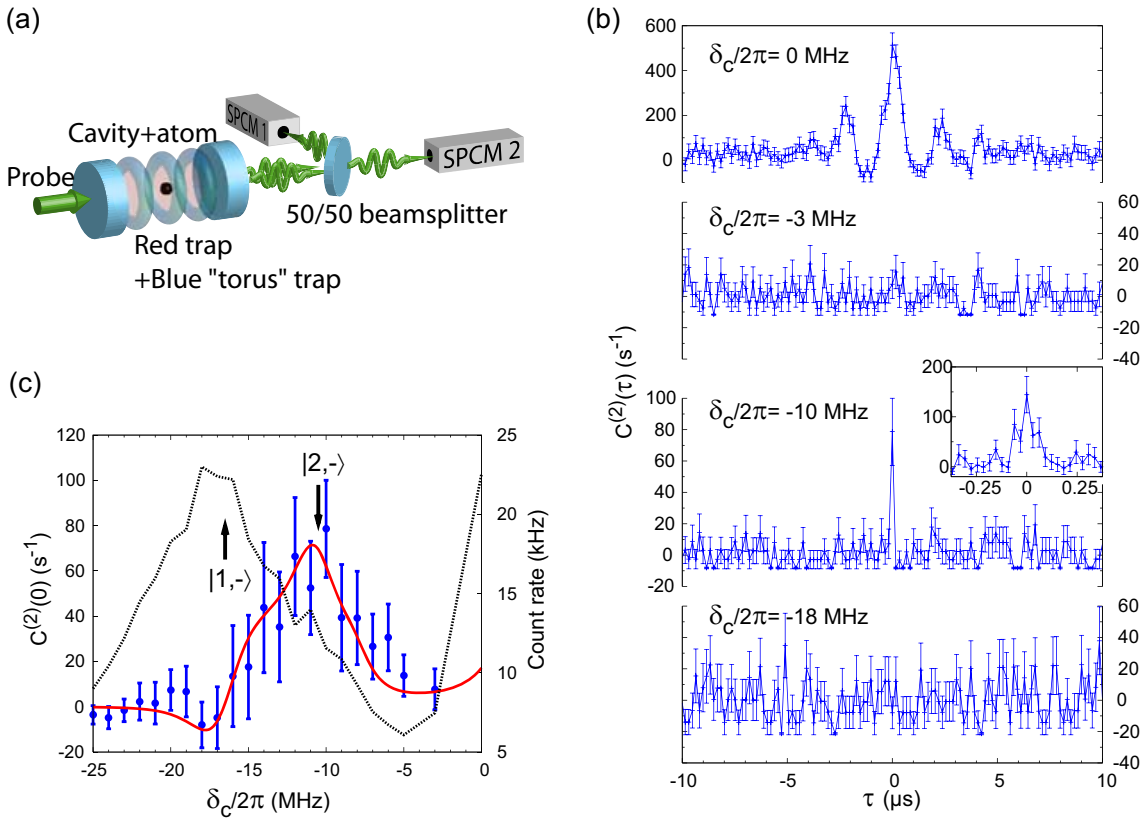

Figure 3.3: Correlations between photons transmitted through the atom-cavity system. (a) Experimental setup: the flux of photons transmitted through the cavity is divided on a 50/50 beamsplitter and sent to two single photon counting modules (SPCMs). (b) Time-dependent correlations $C^{(2)}(\tau)$ for four different probe-cavity detunings δ_c, with an average coupling $g/2\pi = 12$ MHz and an atom-cavity detuning $\delta_{ac}/2\pi = -8.5$ MHz resulting from a "bare" detuning of -35 MHz partially compensated by a 26.5 MHz light shift induced by the dipole traps. On the cavity resonance, the signal is dominated by classical correlations du to atomic motion in the trap. This effect disappears for $|\delta_c| > \gamma$, and a zero-delay correlation peak appears on the two-photon resonance at $\delta_c/2\pi = -10$ MHz (enlarged in the inset). (c) Zero-delay correlations $C^{(2)}(0)$ as a function of probe-cavity detuning (blue circles), fitted with a master-equation model taking into account a finite-width distribution of couplings g due to atomic motion. The black dashed line is the total transmitted photon flux, showing a maximum on the atom-like normal mode $|1,-\rangle$ and a secondary peak on the two-photon resonance with the state $|2,-\rangle$, where $C^{(2)}(0)$ is maximal.

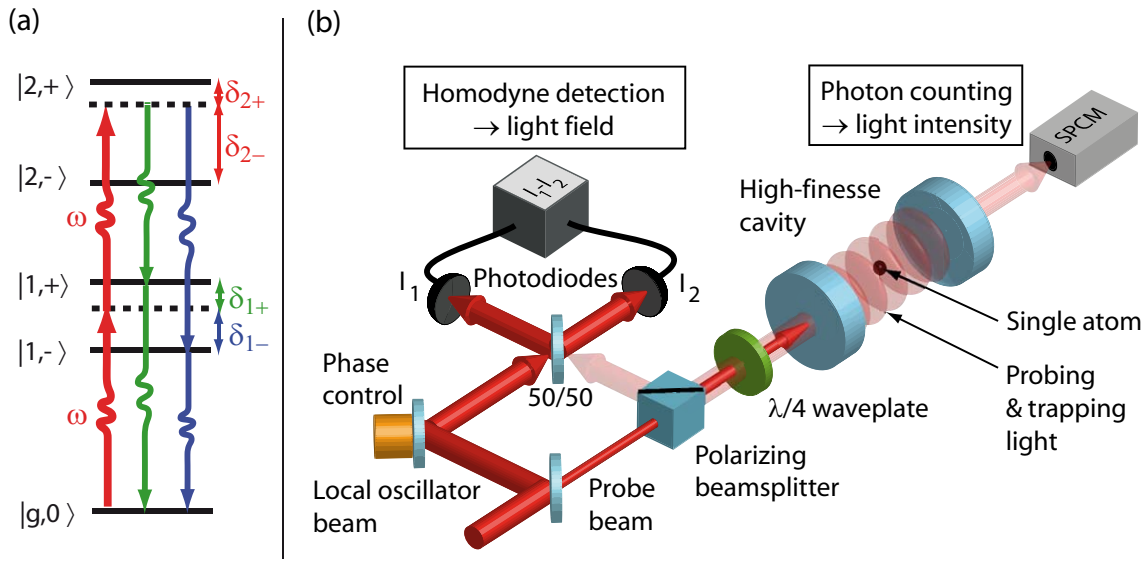

Figure 3.4: (a) When the coupled atom-cavity system is excited with two photons at a frequency ω, detuned by $\delta_{2\pm}$ from the states $|2,\pm\rangle$, it is expected to decay via one of the normal modes $|1,\pm\rangle$, emitting two photons frequency-shifted by $\pm\delta_{1+}$ or $\pm\delta_{1-}$. For each decay channel, correlated quantum fluctuations of the two emitted fields result in quadrature squeezing. (b) Experimental setup. The transmitted intensity is measured with a photon counter for monitoring purposes, while the field reflected from the cavity is measured with a balanced phase-stabilized homodyne detector and sampled with a 14-bit resolution at a 100 MHz rate.

- Does the non-linearity preserve the coherence of the probe, or do the excited multi-photon states decay via a spontaneous, phase-independent cascade?
- Does this lead to quantum coherent effects, such as quadrature squeezing of the emitted light?

As the shifts $\delta_{1,\pm}$ are of the order of 10 MHz in our case, answering the first question requires a spectroscopic analysis with a MHz resolution, a single-photon sensitivity, and low losses to avoid further degrading the experimental duty cycle (see section 3.4). The second and third points above require a phase-sensitive, shot-noise-limited detection.

To tackle all these problems at once, we decided to perform a homodyne spectroscopy of the light leaking out of the cavity, using a setup shown on Fig.3.4. The cavity's transmission was still measured by a photon counter to monitor the atom's coupling, while the beam reflected from the cavity was measured with a phase-stabilized, shot-noise-limited balanced homodyne detector and sampled with a high-resolution fast digitizer. We could then autocorrelate the acquired time-resolved data, or Fourier-transform it to obtain the noise spectrum of the measured quadrature operator

$$\hat{X}_\theta = \frac{\hat{a}e^{i\theta} + \hat{a}^\dagger e^{-i\theta}}{\sqrt{2}} = \hat{X}\cos(\theta) + \hat{P}\sin(\theta), \tag{3.11}$$

where $\hat{a}$ is the photon annihilation operator in the measured mode and the local oscillator's phase θ is actively stabilized using auxiliary beams.

To understand the emitted light's properties, let us first consider a single atom in free space. Because they are widely used as single-photon sources, one often forgets that light

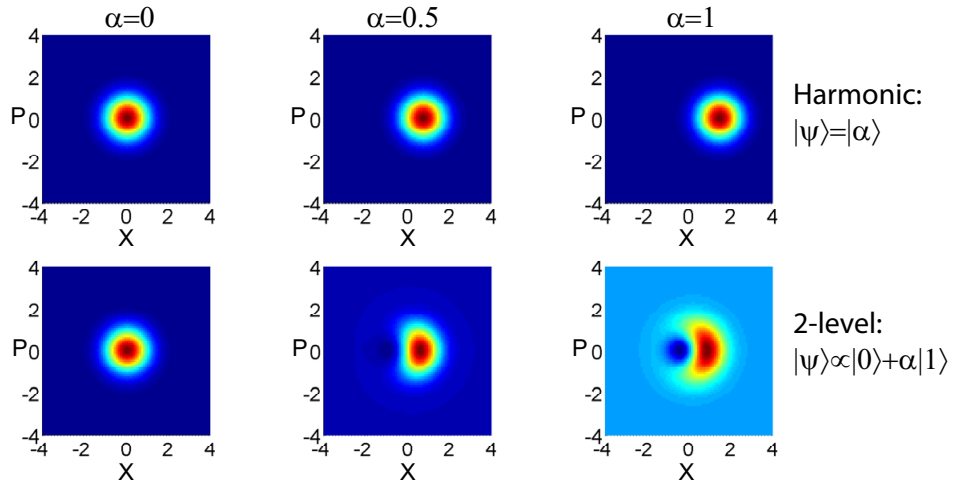

Figure 3.5: A semi-qualitative phase-space picture explaining why light scattered by a single atom can be quadrature-squeezed. A coherently driven harmonic system (top) scatters a coherent state $|\alpha\rangle$, with a symmetric Gaussian Wigner function centered on $X = \alpha\sqrt{2}$. A two-level atom, on the other hand, cannot scatter more than one photon: when the driving increases, the Wigner function becomes squeezed, then "bends" and evolves towards the characteristic single-photon shape.

scattered by single atoms can be squeezed not only in intensity but also in quadratures. This quadrature squeezing, theoretically predicted more than 30 years ago [53, 54], has a rather simple qualitative explanation. First, the atomic response to a weak coherent driving remains coherent. If the atom had a harmonic level structure, it would scatter a coherent state $|\beta\rangle$ proportional to the driving strength α. But because the atom has only two accessible states $|g\rangle$ and $|e\rangle$, the scattered state is "truncated" to one photon at most: $|\psi\rangle = (|0\rangle + \beta\,|1\rangle)/\sqrt{1+|\beta|^2}$. Defining $\Delta\hat{a} = \hat{a} - \langle\hat{a}\rangle$ and assuming $\beta > 0$ for simplicity, the normally-ordered quadrature variance is then

$$\langle :\Delta X_\theta^2: \rangle \;=\; \mathrm{Re}(\langle\Delta\hat{a}^2\rangle e^{2i\theta}) + \langle\Delta\hat{a}^\dagger\Delta\hat{a}\rangle = -\frac{\beta^2\cos(2\theta)}{(1+\beta^2)^2} + \frac{\beta^4}{(1+\beta^2)^2}. \qquad (3.12)$$

For $\beta^2 < \cos(2\theta)$, $\langle :\Delta X_\theta^2: \rangle$ becomes negative and the beam is quadrature-squeezed (Fig.3.5). In a more rigorous, master-equation-based approach, one can use the fact that light scattered by the atomic dipole obeys $\Delta\hat{a} \propto \Delta\hat{\sigma}$, so, for a weak driving α, $\langle\Delta\hat{a}^2\rangle \propto \langle\Delta\hat{\sigma}^2\rangle = -\langle\hat{\sigma}\rangle^2 \propto \alpha^2$. A more involved calculation shows that the incoherent term $\langle\Delta\hat{a}^\dagger\Delta\hat{a}\rangle$ still scales as α^4 and can be neglected, allowing $\langle :\Delta X_\theta^2: \rangle \approx \mathrm{Re}(\langle\Delta\hat{a}^2\rangle e^{2i\theta})$ to become negative for a properly chosen phase.

Qualitative changes appear when the atom is strongly coupled to a cavity. Solving the master equation to the lowest order in α, one still gets $\langle :\Delta X_\theta^2: \rangle \approx \mathrm{Re}(\langle\Delta\hat{a}^2\rangle e^{2i\theta})$ and, more explicitly,

$$\langle :\Delta X_\theta^2: \rangle \;=\; -\mathrm{Re}(K\langle\hat{\sigma}\rangle^2 e^{2i\theta}), \qquad (3.13)$$

$$\langle\hat{\sigma}\rangle \;=\; \frac{\alpha g}{\Delta_{1+}\Delta_{1-}}, \qquad (3.14)$$

$$K \;=\; \frac{2g^2}{\Delta_{2+}\Delta_{2-}}. \qquad (3.15)$$

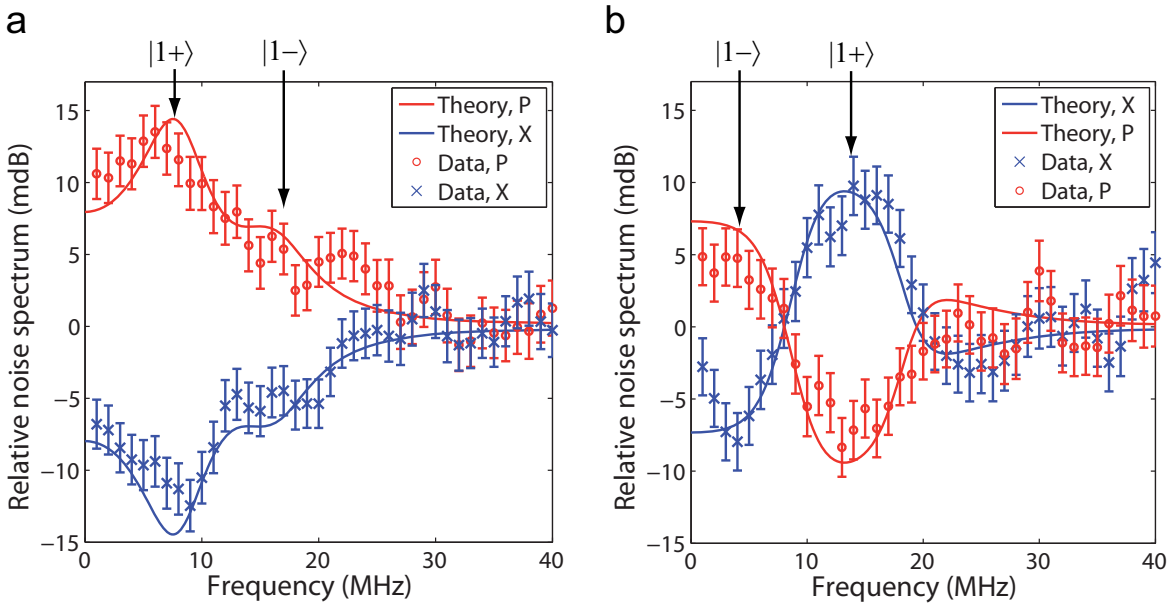

Figure 3.6: Measured quadrature squeezing spectra of light reflected by the atom-cavity system. (a) When the probe is resonant with the cavity and detuned from the atom by $\delta_a/2\pi = 8$ MHz, the system mainly decays via the state $|1,+\rangle$, leading to a 12 mDb squeezing dip on the X quadrature around $\Omega \approx \delta_{1+} \approx 2\pi \times 9$ MHz, with a shoulder around $\Omega \approx \delta_{1-} \approx 2\pi \times 15$ MHz corresponding to the off-resonant decay via $|1,-\rangle$. (b) Close to the two-photon resonance with the state $|2,-\rangle$ ($\delta_c/2\pi = -12$ MHz, $\delta_a/2\pi = 3$ MHz), the two decay channels have comparable strengths ans interfere destructively: the decay via $|1,-\rangle$ leads to squeezing of $X = X_0$, while the decay via $|1,+\rangle$ squeezes $P = X_{\pi/2}$.

The factor $-\langle\hat{\sigma}\rangle^2$ corresponds to free-space squeezing involving only single-photon physics. In contrast, the factor K, specific to the strong coupling regime, depends on the complex detunings of the two-photon-exited states. Moreover, the cavity qualitatively changes the photon statistics: quadrature-squeezed light scattered by a free-space atom remains antibunched, whereas the atom-cavity system driven on the two-photon transition emits bunched quadrature-squeezed light. The squeezing spectrum S outside the cavity, normalized to the shot noise and including the detection efficiency η, can be obtained by Fourier-transforming the field autocorrelation function $\langle : \Delta X_\theta(\tau)\Delta X_\theta(0) : \rangle$ calculated using the quantum regression theorem:

$$S_\theta(\Omega) = 1 + \eta 2\kappa \int_0^\infty d\tau \cos(\Omega\tau)\langle : \Delta X_\theta(\tau)\Delta X_\theta(0) : \rangle \tag{3.16}$$

$$= 1 + 8\eta\kappa \mathrm{Re}\left\{ e^{-2i\theta}\langle \Delta a^2 \rangle \frac{i\Delta_{1+}\Delta_{1-}}{\Delta_{1+} - \Delta_{1-}} \left(\frac{1}{\Omega^2 - \Delta_{1-}^2} - \frac{1}{\Omega^2 - \Delta_{1+}^2} \right) \right\}, \tag{3.17}$$

Experimental squeezing spectra shown on Fig.3.6, consistently interpolated by this model taking into account the detector's response, depend on the probe-cavity detuning δ_c. When the probe is resonant with the empty cavity and detuned from the atom, the system mainly decays via the state $|1,+\rangle$, leading to a squeezing dip on the X quadrature around $\Omega \approx \delta_{1+}$. In contrast, close to the two-photon resonance with the state $|2,-\rangle$ the two decay processes have comparable amplitudes and opposite phases: the decay via

$|1,-\rangle$ leads to squeezing of $X = X_0$, while the decay via $|1,+\rangle$ squeezes $P = X_{\pi/2}$.

Compared to $>$ 10 dB squeezing levels which can now be achieved in parametric systems, the 12mDb squeezing produced here is tiny. However, while parametric amplifiers require watts of pumping power, this system operates with an impinging probe power of only 8 nW, corresponding to ~ 2 photons per system's decay time. At higher probe powers it rapidly saturates, but the lowest-order dispersive $\chi^{(3)}$ non-linearity exceeds by seven orders of magnitude that of a standard single-mode optical fibre with the same amount of losses [3] and by four orders of magnitude the $\chi^{(3)}$ obtained by four-wave mixing in macroscopic atomic systems with similar bandwidths [55]. Unfortunately, another four orders of magnitude are missing for this system to be used for deterministic quantum logic between optical qubits. The problem does not come from the physical mechanism (which works efficiently in the microwave domain) but from the parameter regime, which requires two quantitative improvements:

- Increase the single-atom cooperativity $C_0 = g^2/2\kappa\gamma$.
- Operate in the "bad cavity" limit, so that the system predominantly decays by emitting photons through the input/output coupler of the cavity.

In other words, one needs to go from $g > \gamma > \kappa$ in current experiments to the regime where $g \gg \kappa \gg \gamma$. Achieving this may require a different technological implementation, as will be discussed in section 3.5.

3.4 Feedback cooling of a single atom

For publications related to this section, see Appendix **??**,**??** *or Refs. [56, 57, 58]*

In addition to improving the "physical" parameters above, one problematic point we had to address was the dynamic control of the atom-cavity coupling. For a typical acquisition performed on our "old" setup,

- it took $\approx$ 3s to load the MOT and launch the atomic cloud,
- an atom was captured only one time out of 10,
- the captured atom remained strongly coupled to the cavity for only $\approx$ 1 ms.

Adding maintenance downtime, we typically obtained $\approx$ 4 seconds of useful data per week of full-time acquisition: even if the physical mechanism could lead to deterministic photonic interactions in principle, an experiment with a duty cycle of $\sim 10^{-6}$ could hardly be called "scalable". Improving the storage time of the atom in the cavity and maintaining it strongly coupled to the probe mode was therefore a crucial problem.

The main process heating trapped atoms and expelling them from the trap was the scattering of probe photons: while an atom could remain trapped "in the dark" for $\sim$ 100 ms (when other effects, such as parametric heating by the fluctuations of the dipole trap, came into play), typical probe powers reduced this time down to a few ms at most. Oscillations along the cavity axis could be efficiently damped by cavity cooling [59, 60, 45, 61], but radial motion could not be reduced by standard laser cooling techniques because of the limited optical access to our small-volume cavity.

To address this issue, we proposed and demonstrated an active feedback cooling protocol, by measuring the coupling-dependent cavity transmission and reacting on the trapping potential's depth. Compared to previous experiments on feedback cooling of single ions [62] or single electrons [63], our protocol had to satisfy several constraints specific to our system:

- Our maximal trapping potential is only ~ 1 mK, many orders of magnitude weaker than electrostatic traps $100 - 1000$ K deep.
- We have to cool motion in all three spatial dimensions rather than only one.
- By doing this, we should avoid heating one degree of freedom while cooling another. In particular, because axial oscillations happen at frequencies around 500 kHz, ~ 100 times faster than the radial ones, they are too fast to be feedback-cooled, so a switching trapping potential cooling radial oscillations may be seen as random noise increasing axial ones.
- We must prevent the atom from revolving on azimuthal trajectories at a given distance from the cavity axis, as these trajectories do not result in a modulation of the photonic flux.
- The atomic motion is very chaotic and decoheres at the timescale of half an oscillation (see correlation measurements at $\delta_c = 0$ on Fig.3.3). This excludes the possibility of integrating signal over several oscillation periods and requires a real-time feedback strategy.
- Trapped atoms have wide distributions of kinetic energies and may perform large excursions away from the cavity axis, where the trap becomes anharmonic. This means that we cannot modulate its depth with a fixed frequency but have to control it in real time.
- The feedback loop must operate at least 10 times faster than the ~ 100 μs decoherence time of radial motion. Besides fast digital electronics, this requires a photon count rate of 100 kHz at least to provide a meaningful signal to react on.
- Unfortunately, while a brighter probe increases the feedback signal it also heats the atoms. In our setup, a 100 kHz photon count rate corresponds to ~ 0.1 intracavity photons in the steady state and a comparable population of the atomic excited state, leading to a heating rate sufficient to expel the atom from the trap within a few tens of milliseconds. The probe power must therefore be kept to an acceptable minimum and the feedback cooling mechanism must be efficient.

Our feedback protocol is described on Fig.3.7. Like previously, we chose an effective cavity-atom detuning of the same order as the maximal cavity-atom coupling and tuned the probe on the empty cavity resonance. Besides an efficient cavity-cooling of axial oscillations, this regime was optimal for detecting radial atomic motion: an atom moving away from the cavity axis led to a strong and monotonous increase of the transmitted photon flux. This was detected by a FPGA-based logic circuit, triggering an increase of the dipole potential preventing the atom from escaping the trap. When the atom started

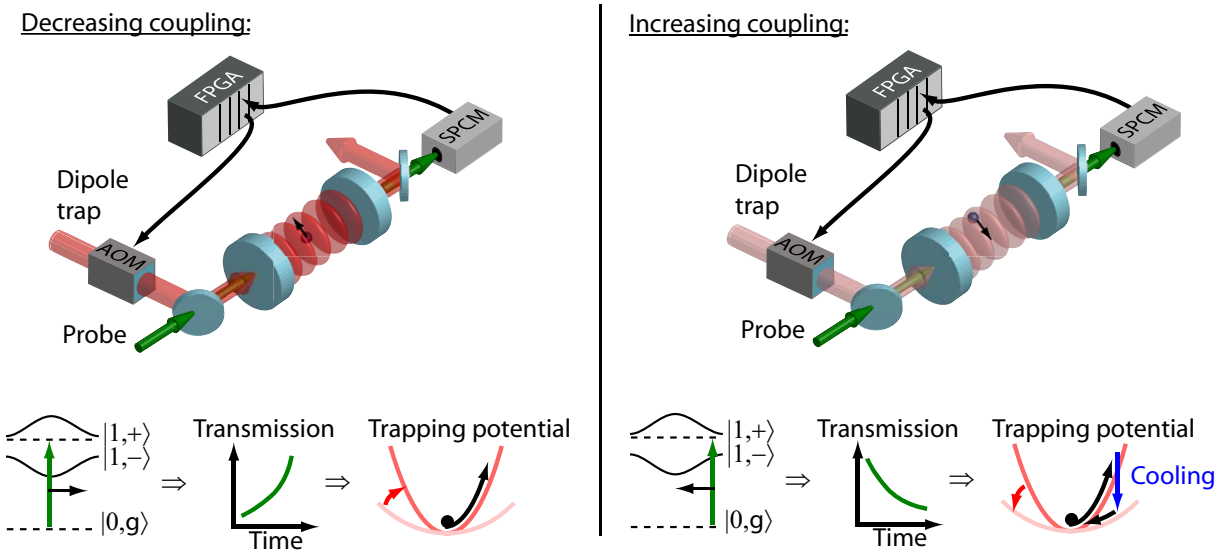

Figure 3.7: Cooling the radial motion of a single atom inside a high-finesse cavity by active feedback. When the atom moves away from the cavity axis the coupling decreases. In our parameter regime ($\delta_c = 0$, $\delta_a/2\pi = 20$ MHz), this brings the cavity-like state $|1,+\rangle$ closer to resonance with the probe, which results in a strong and monotonic increase of the transmitted photonic flux. This is detected by a FPGA-based logic circuit which acts on an acousto-optical modulator to increase the dipole trap's power and prevent the atom from escaping. When the atom moves back towards the cavity axis the photonic flux decreases and the logic circuit rapidly lowers the trapping potential, thus removing energy from the system after half an oscillation cycle.

moving back towards the cavity axis, the logic circuit rapidly decreased the trapping potential, thus removing energy from the system after half an oscillation cycle.

In our first implementation of this protocol on the "old" setup [56, 58, 48], the feedback loop had an overall delay time of 3 μs, and the probe was weak enough for the decision-making process to be based on single photon detection events. We kept the "red" trap constant and switched the repulsive "torus" between a low and a high intensity, thus only acting on radial motion and leaving axial cavity cooling undisturbed. In addition, because atoms mostly remained near the cavity axis where the torus intensity was low, switching this torus had little effect on atomic AC Stark shifts and thus did not directly modify the cavity transmission: in other words, this removed spurious couplings between the "observation" and the "reaction" parts of the feedback loop. The X and Y components of the torus had different intensities to break the circular symmetry and make azimuthal trajectories unstable. An optimally-chosen 10 μs photon-counting integration time allowed us to increase the average atomic storage time from 3 ms to 8 ms, further improved to 25 ms by adding a repumper beam (bringing atoms which decayed to the $5S_{1/2}, F = 2$ manifold back to the probed transition) and a second loop in the feedback protocol which made it react more slowly to decreasing photon fluxes than to increasing ones.

We transposed this feedback cooling technique to the "new" setup, where the red-detuned attractive trap was the only available [57, 49]. This drawback was largely compensated by a much better photon detection efficiency: an intracavity photon had a 20% chance to be detected, compared to 4% in the first experiment. This strongly increased the signal to noise ratio of the feedback loop, allowing us to trap an atom for $> 1s$ on average and to reduce its temperature from 400 to 160 μK. The cooling is limited by the non-linear dependence of the transmitted photonic flux on the atomic position: atoms located within a few μm from the cavity axis decrease the transmission to almost zero, and their oscillations become undetectable.

Although it is not as efficient as laser cooling, feedback cooling preserves the internal state of the atom and can be used in systems with a limited optical access, which is typical in CQED. On the "new" setup, feedback cooling became a practical tool for extending atomic storage times and increasing average couplings. It is used on a daily basis in experiments which would be impossible otherwise.

3.5 Outlook

Since I left the MPQ in 2009, the field of CQED evolved dramatically. The revolution came from circuit QED which became a leading technology for quantum information processing (QIP) and quantum simulations. Currently, only trapped ions allow one to implement comparably complex protocols, leaving all other technologies behind. Optical photons remain nevertheless the only candidates to transmit quantum states over long distances, and experiments at optical wavelengths keep several technical advantages such as the possibility to count individual photons with a high efficiency. In this context, Fabry-Pérot resonators using "bulk" mirrors made quantitative progress in terms of control and flexibility, leading to more complex experiments with multiple photons [64] or multiple atoms [65]. They have also been made more compact by imprinting mirrors on optical fiber ends [66]. A very interesting and increasingly popular alternative to Fabry-Pérot cavities consists in coupling atoms to evanescent fields of dielectric microresonators in different

shapes: bottle-like optical fibers [67], microtores [42, 68], photonic crystal cavities [69], etc. They have very high quality factors, low scattering losses, and their strongly confined evanescent fields lead to large couplings with single atoms. In parallel to these experiments where atomic motion remains a serious issue, solid-state systems based on quantum dots coupled to semiconductor nano-cavities made significant progress and can now reach non-linearities significant at a few photons level [70, 71, 17]. Here, the main current bottleneck is the control of the environment: fabrication processes are not precise enough to produce two identical devices capable of producing indistinguishable photons.

Overall, CQED is still the most widespread approach for deterministic photon-photon interactions. It has been making steady progress during the last few decades and it now performs remarkably well in the microwave domain. At optical wavelengths, many problems may seem somewhat "technical" but solving them often leads to unexpected and interesting physics.

Chapter 4

Interactions of optical photons in Rydberg atomic ensembles

Contents

4.1 Introduction 32
4.2 Experimental setup 34
4.3 Non-linear dispersion of a Rydberg gas 36
4.3.1 Effective master and Bloch equations 36
4.3.2 Dipole blockade model 37
4.3.3 Experiment 38
4.3.4 Conclusion: strength of the non-linearity 40
4.4 Homodyne tomography of a single photon retrieved from an atomic memory 41
4.4.1 Experimental protocol 41
4.4.2 Results 42
4.5 Few-photon interactions in a Rydberg gas 42
4.5.1 Theoretical models 44
4.5.2 Current direction: converting losses into phase shifts 46

4.1 Introduction

Atoms excited to high-lying "Rydberg" states have many remarkable properties [72]. Because they are nearly ionized, with one highly excited electron and an inner electron shell, they can be rather accurately described by a hydrogen-like model with an effective principal quantum number $n^* = n - \delta$ where δ is a state-dependent quantum defect. It is then easy to derive orders of magnitude and scaling laws for several quantities of interest for quantum information science [73]:

- Their transition frequencies between neighboring states scale as n^{*-3} and fall in the microwave domain for $n \sim 50 - 100$, the typical range of principal quantum numbers used in experiments.

- The corresponding transition dipoles $d \sim n^{*2} e a_0$ where e is the elementary charge and a_0 is the Bohr radius typically exceed by three orders of magnitude those of usual polar molecules such as water.

- Their natural lifetimes scale as n^{*3} (for low orbital angular momentum states) to n^{*5} (for "circular" states with high orbital angular momentum) and reach the millisecond range, reduced to $\sim 100\ \mu s$ by thermal photons in room-temperature experiments. As for the corresponding excitation linewidths, they are generally broadened by experimental noise to ~ 100 kHz.

- Their static polarizabilities increase as n^{*7}, making them very sensitive to DC electric fields [74, 75].

- Their van-der-Waals interactions scale as n^{*11} and may exceed all decoherence rates for two atoms located several tens of microns apart, a very large distance compared to the ~ 10 nm scattering length for ground-state atomic collisions. This distance can be increased further by tuning these interactions into the resonant dipole-dipole regime using applied electric or microwave fields.

The first three points imply that these atoms can be very strongly coupled to microwave photons, which lies at the basis of on-going microwave CQED experiments pioneered in the 1980's by Herbert Walter in Garching and by Serge Haroche in Paris [11]. The last one sparked a lot of interest in the QIP community a decade ago, with a proposal to use long-range interactions between Rydberg atoms to implement multi-qubit logic gates in an atomic quantum register [76]. Experiments successfully moving along this line are now led by Mark Saffman in Madison, Immanuel Bloch in Munich and Antoine Browaeys in Palaiseau.

Using the same effect to create strong interactions between optical photons [77] was proposed by Friedler *et al* [21]. The idea, already introduced in Chap. 1, consisted in injecting photons in an optically dense atomic cloud, creating electromagnetically-induced transparency (EIT) with a "control" laser which converts these photons into slow Rydberg polarisation waves, and using interactions between these Rydberg polaritons to induce the desired non-linear effect. Several pioneering experiments in the group of Charles Adams in Durham [78, 22] gave hope that this approach could bring deterministic photonic interactions within experimental reach. In 2009 I joined the CNRS as a staff scientist to develop a new project along these lines in the group of Philippe Grangier in Palaiseau. Around the same time, similar projects started in many other groups: Alex Kuzmich in GeorgiaTech [79, 80, 81, 82], Vladan Vuletić in Harvard collaborating with Mikhail Lukin in MIT [83, 84], Matthias Weidemüller in Heidelberg [85], Sebastian Hofferberth in Stuttgart [86]...

When I moved to Palaiseau, doing quantum optics in a Rydberg gas was still a new idea, with very little experimental and theoretical knowledge available. We started with an empty lab, good funding but no equipment, and no reliable experimentally-validated theoretical models to guide our first steps. We knew, however, that we had to go beyond a proof-of-principle demonstration of photonic interactions: for most applications in QIP, we also had to show that these interactions can occur with little losses and that all photonic properties (temporal profile, spatial mode, frequency, polarisation...) can be kept under

control throughout the process. This led us to designing a setup with two distinctive features:

- A low-finesse cavity surrounding the atomic cloud, to enhance non-linear effects and to control spatial and spectral photonic modes,
- A homodyne detection setup, to measure non-linear interaction-induced phase shifts and to perform full single-mode quantum tomographies of light states emitted from the system.

Considered that combining quantum optics, cold atoms and many-body interacting quantum systems in a same experiment was a challenging task, we decided to organize the project as follows:

- Design and build the core of the experimental setup, consisting in a cold atomic cloud trapped inside a low-finesse Fabry-Perot optical cavity, together with the required laser bench, stabilization electronics, and control & acquisition system. From my past experience I estimated that each of these four sub-systems (vacuum, optics, electronics and informatics) would take approximately six months to be completed, which proved to be correct.
- Observe and model dispersive optical interaction-induced non-linearities in a cold Rydberg gaz in a classical regime, without concerns about quantum effects. This was done in 2012, when most of the setup was assembled (see section 4.3).
- Then do the opposite and leave Rydberg physics aside for a time, to verify whether a non-classical state prepared in the atomic gas can be efficiently retrieved as a single-mode free-propagating optical pulse and characterized with our detection tools. We demonstrated this experimentally in 2013 (section 4.4).
- Finally, combine both quantum optics and Rydberg physics to create deterministic and efficient photonic interactions with little losses (section 4.5).

Besides published articles, a detailed account of this work can be found in Erwan Bimbard's PhD thesis which I co-supervised from 2011 to 2014.

4.2 Experimental setup

We started our experiments by loading a cloud of ^{87}Rb atoms in a magneto-optical trap (MOT) and cooling it down to $\approx 50\ \mu K$ using optical molasses. The trap was formed inside a single-ended Fabry-Pérot cavity with a 5% input-output coupler transmission and a ~ 65 mm length. This length was tunable over a few mm to bring a set of TEM_{00} modes close to resonance with selected atomic transitions, while other spatial modes remained far-detuned and could be ignored. The mode coupled to the stretched atomic transition $5S_{1/2}, F = 2, m_F = 2 \rightarrow 5P_{3/2}, F = 3, m_F = 3$ had a waist of 86 μm, leading to a maximal single-atom coupling rate $g/2\pi = 0.24$ MHz considerably smaller than the atomic dipole decay rate $\gamma_e/2\pi = 3$ MHz or the cavity field decay rate $\gamma_c/2\pi = 10$ MHz. By adjusting the number N of atoms coupled to the cavity, we obtained collective cooperativities $C = Ng^2/2\kappa\gamma \approx N/1000$ ranging between 5 and 250 in practice. Beams

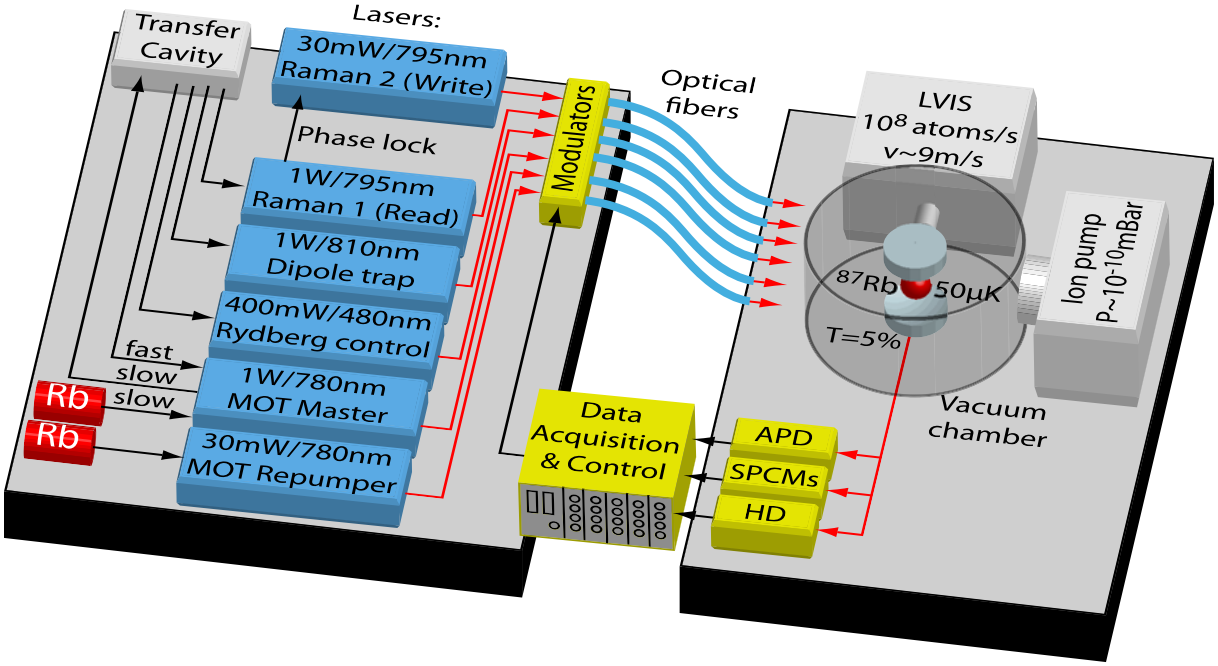

Figure 4.1: Experimental setup designed and built in the Institut d'Optique to study Rydberg-mediated photonic interactions. The laser bench (left) contains six lasers creating ~ 15 independent beams controlled by acousto-optical and electro-optical modulators. At low frequencies, the MOT master and repumper lasers are frequency-locked on Doppler-free saturated absorption lines in Rb vapor cells. The MOT master laser stabilizes slow drifts of the transfer cavity, which then provides an absolute frequency reference for all other lasers stabilized to a $20-80$ kHz precision. These laser beams are used to trap, cool and excite a cold cloud of ^{87}Rb atoms trapped inside a low-finesse single-ended Fabry-Perot cavity placed under ultra-high vacuum. The atomic cloud is loaded from a custom-made Low Velocity Intense Source (LVIS, [87]). Light transmitted through the cavity's input/output coupler (transmission $T = 5\%$) is directed to an avalanche photodiode (APD), a set of single photon counting modules (SPCMs), or a balanced shot-noise-limited homodyne detector (HD). A PXI-based system creates dynamic control sequences with a 10 ns time resolution and acquires digital and analog signals with $100-250$ MHz sampling rates. See text for details.

required to trap, cool, excite and probe the atoms were delivered through optical fibers from a separate optical bench containing six frequency-stabilized lasers. Light emitted from the cavity could be detected by an avalanche photodiode operating in the linear regime, a set of single photon counting modules (SPCMs) and/or a shot-noise-limited balanced homodyne detector. The experimental setup is sketched on Fig.4.1.

4.3 Non-linear dispersion of a Rydberg gas

For publications related to this section, see Appendix **??**,**??** *or Refs. [88, 89]*

Our first goal was to measure an intensity-dependent phase shift induced by atomic interactions on a probe beam injected in the cavity. This experiment allowed us to develop first reliable theoretical models specific to our system.

4.3.1 Effective master and Bloch equations

To a good approximation, we can consider our system as an ensemble of N three-level atoms with a ground state $|g\rangle$, and intermediate state $|e\rangle$ and a highly excited Rydberg state $|r\rangle$. The lower transition $|g\rangle \rightarrow |e\rangle$ couples with a constant g to a cavity mode driven by a weak coherent probe with an amplitude α, while the upper transition $|e\rangle \rightarrow |r\rangle$ is driven by a control field with a Rabi frequency Ω_b. The system can then be described in the rotating wave approximation by the master equation

$$\frac{\mathrm{d}\hat{\rho}}{\mathrm{d}t} = -i[\hat{H},\hat{\rho}] + \mathcal{L}\hat{\rho}, \tag{4.1a}$$

$$\begin{aligned}\hat{H} &= -\delta_c \hat{a}^\dagger \hat{a} + \sum_{j=1}^{N}\left(-\delta_e \hat{\sigma}_{ee}^{(j)} - \delta_r \hat{\sigma}_{rr}^{(j)} + g(\hat{a}^\dagger \hat{\sigma}_{ge}^{(j)} + \hat{a}\hat{\sigma}_{eg}^{(j)}) + \frac{\Omega_b}{2}(\hat{\sigma}_{er}^{(j)} + \hat{\sigma}_{re}^{(j)})\right) \\ &\quad + \sum_{i<j} \kappa_{ij} \hat{\sigma}_{rr}^{(i)} \hat{\sigma}_{rr}^{(j)} + \alpha(\hat{a} + \hat{a}^\dagger),\end{aligned} \tag{4.1b}$$

$$\begin{aligned}\mathcal{L}\hat{\rho} &= \gamma_c(2\hat{a}\hat{\rho}\hat{a}^\dagger - \hat{a}^\dagger\hat{a}\hat{\rho} - \hat{\rho}\hat{a}^\dagger\hat{a}) + \sum_{j=1}^{N}\big(\gamma_e(2\hat{\sigma}_{ge}^{(j)}\hat{\rho}\hat{\sigma}_{eg}^{(j)} - \hat{\sigma}_{ee}^{(j)}\hat{\rho} - \hat{\rho}\hat{\sigma}_{ee}^{(j)}) \\ &\quad + \gamma_r(2\hat{\sigma}_{gr}^{(j)}\hat{\rho}\hat{\sigma}_{rg}^{(j)} - \hat{\sigma}_{rr}^{(j)}\hat{\rho} - \hat{\rho}\hat{\sigma}_{rr}^{(j)}) + \gamma_r'(2\hat{\sigma}_{rr}^{(j)}\hat{\rho}\hat{\sigma}_{rr}^{(j)} - \hat{\sigma}_{rr}^{(j)}\hat{\rho} - \hat{\rho}\hat{\sigma}_{rr}^{(j)})\big).\end{aligned} \tag{4.1c}$$

Here $\hat{\sigma}_{kl}^{(j)} = |k\rangle_j \langle l|_j$ for the j-th atom, $\hat{a}$ is the annihilation operator in the cavity mode, $\delta_c = \omega - \omega_c$ is the probe-cavity detuning, $\delta_e = \omega - \omega_{ge}$ is the detuning of the probe from the $|g\rangle \rightarrow |e\rangle$ resonance, and $\delta_r = \omega + \omega_b - \omega_{gr}$ is the two-photon detuning from the $|g\rangle \rightarrow |r\rangle$ transition. As for the incoherent part of the evolution, aside from the cavity field decay rate γ_c and the respective natural linewidths γ_e and γ_r of the intermediate and Rydberg states, the total dephasing rate $\gamma_d = \gamma_r + \gamma_r'$ of the ground-Rydberg coherence is generally dominated by the inhomogeneous environment-induced term γ_r'.

We generally consider probe powers low enough to assume $\langle\hat{\sigma}_{ee}\rangle \ll 1$ and $\langle\hat{\sigma}_{rr}\rangle \ll 1$. Non-linear effects are then only due to interactions between Rydberg atoms introduced via the couplings κ_{ij}, which depend in general not only on the distance R_{ij} between the atoms i and j but also on the angle between their inter-nuclear axis and the light's polarisation.

Because our atoms are randomly positioned this angular dependence is averaged out in our models, to describe these interactions by a single effective van-der-Waals potential $\kappa_{ij} = -C_6/R_{ij}^6$. Despite these simplifications, this system involving thousands of interacting atoms remains too complex for an exact numerical integration.

In the classical limit, one can further simplify the problem and assume that the cavity contains a classical field driving the lower atomic transition with a Rabi frequency Ω. One can then introduce complex detunings $\Delta_e = \delta_e + i\gamma_e$ and $\Delta_r = \delta_r + i\gamma_d$ to derive a set of Bloch equations describing the dynamics of single-atom expectation values $\sigma_{kl} = \langle\hat{\sigma}_{kl}^{(i)}\rangle$:

$$i\frac{\mathrm{d}\sigma_{ge}}{\mathrm{d}t} = -\Delta_e\sigma_{ge} + \frac{\Omega}{2}(1 - 2\sigma_{ee} - \sigma_{rr}) + \frac{\Omega_b}{2}\sigma_{gr} \tag{4.2a}$$

$$i\frac{\mathrm{d}\sigma_{gr}}{\mathrm{d}t} = -\Delta_r\sigma_{gr} + \frac{\Omega_b}{2}\sigma_{ge} - \frac{\Omega}{2}\sigma_{er} + \sum_{j\neq i}\kappa_{ij}\langle\hat{\sigma}_{gr}^{(i)}\hat{\sigma}_{rr}^{(j)}\rangle, \tag{4.2b}$$

$$i\frac{\mathrm{d}\sigma_{er}}{\mathrm{d}t} = -(\Delta_r - \Delta_e^*)\sigma_{er} + \frac{\Omega_b}{2}(\sigma_{ee} - \sigma_{rr}) - \frac{\Omega}{2}\sigma_{gr} + \sum_{j\neq i}\kappa_{ij}\langle\hat{\sigma}_{er}^{(i)}\hat{\sigma}_{rr}^{(j)}\rangle, \tag{4.2c}$$

$$\frac{\mathrm{d}\sigma_{ee}}{\mathrm{d}t} = -2\gamma_e\sigma_{ee} + \Omega_b\mathrm{Im}(\sigma_{er}) - \Omega\mathrm{Im}(\sigma_{ge}), \tag{4.2d}$$

$$\frac{\mathrm{d}\sigma_{rr}}{\mathrm{d}t} = -2\gamma_r\sigma_{rr} - \Omega_b\mathrm{Im}(\sigma_{er}) \tag{4.2e}$$

Due to interactions, they depend on two-body correlation terms $\langle\sigma_{kl}^{(i)}\sigma_{mn}^{(j)}\rangle$ which in turn depend on three-body correlators, etc. This leads to a hierarchy of Bloch equations with increasing complexity, which can only be treated under some approximations.

4.3.2 Dipole blockade model

In the classical regime, the optical response of the atomic cloud can be described by its refractive index, related to the atomic polarizability $\alpha = 2\gamma_e\sigma_{12}/\Omega$. This polarizability can be calculated using the "blockade" model sketched on Fig.1.4, which assumes that each excited Rydberg atom is surrounded by a blockade volume V_b where other atoms are decoupled from the Rydberg state. A "quick and dirty" way of deriving it consists in three steps:

- Solve the optical Bloch equations above to the lowest order in Ω in order to calculate the steady-state linear polarizability

$$\alpha_{3l} = \lim_{\Omega\to 0}(\alpha) = \frac{\gamma_e}{\Delta_e - \Omega_b^2/4\Delta_r} = \frac{\gamma_e}{\widetilde{\Delta}_e} \tag{4.3}$$

  and the Rydberg population

$$\sigma_{rr} = \frac{\Omega^2\Omega_b^2}{16|\widetilde{\Delta}_e|^2|\Delta_r|^2}\frac{\gamma_d + (1+\gamma_d/\gamma_e)\mathrm{Im}[(\Delta_r^* - \Delta_e)^{-1}]\Omega_b^2/4}{\gamma_r + (1+\gamma_r/\gamma_e)\mathrm{Im}[(\Delta_r^* - \Delta_e)^{-1}]\Omega_b^2/4}. \tag{4.4}$$

- To account for interactions, simply assume that an atom i in the Rydberg state changes the complex two-photon detuning of an atom j from Δ_r to $\Delta_r - C_6/R_{ij}^6$. Atoms close to the atom i become uncoupled from the Rydberg state and their polarizability $\alpha(R_{ij})$ tends to the two-level limit $\alpha_{2l} = \gamma_e/\Delta_e$. The effective number of

atoms n_b "blockaded" by a Rydberg excitation can then be calculated in a continuum approximation with an atomic density μ:

$$\int \mu \mathrm{d}^3\mathbf{R}\,(\alpha(R) - \alpha_{3l}) = n_b(\alpha_{2l} - \alpha_{3l}) \tag{4.5}$$

$$\Rightarrow n_b = \mu V_b = \frac{2\pi^2\mu}{3}\sqrt{\frac{C_6}{\Delta_r - \Omega_b^2/4\Delta_e}} = \frac{2\pi^2\mu}{3}\sqrt{\frac{C_6}{\widetilde{\Delta}_r}} \tag{4.6}$$

- In the lowest-order limit where only a small fraction of the cloud is blockaded, this gives a very simple expression for the average polarizability α across the cloud:

$$\alpha = \alpha_{3l} + (\alpha_{2l} - \alpha_{3l})n_b\sigma_{rr} = \alpha_{3l} + (\alpha_{2l} - \alpha_{3l})sY. \tag{4.7}$$

  where Y is the incoming probe power and $s = n_b\frac{\mathrm{d}\sigma_{rr}}{\mathrm{d}Y}(0)$ can be easily expressed knowing the cooperativity C and the normalized cavity detuning δ_c/γ_c.

A more elaborate calculation done by expanding the initial set of Bloch equations in powers of Ω gives the same result [89].

This model is simple enough to include several experimental artifacts, in particular inhomogeneous Rabi frequencies and excitation dynamics: beams injected in the cavity form standing waves with high contrasts, and measurements are generally performed faster than the time it takes to reach the steady state (in fact the steady state predicted by our model is never reached because other phenomena eventually come into play: the atomic cloud falls and expands, Rydberg atoms collide and ionize...). Accounting for these effects still yields analytical albeit cumbersome expressions which can be used to fit actual experimental data.

When the probe power increases, the cloud becomes filled with blockade spheres: the non-linearity deviates from the $\chi^{(3)}$ regime described by Eq.4.7 and eventually saturates. A simple way to account for this is to consider blockade spheres as two-level non-interacting "superatoms" progressively filling all the available volume. Simple optical Bloch equations for "standard" two-level atoms show that their normalized polarizability scales as $1/(1 + s_0X)$ where X is the intracavity intensity and s_0 is nothing else than the coefficient characterizing the lowest-order $\chi^{(3)}$ non-linearity (a result well known in the context of saturated absorption or saturated laser gain). One can transpose this to Rydberg-blockaded "superatoms" and assume that

$$\frac{\alpha - \alpha_{2l}}{\alpha_{3l} - \alpha_{2l}} = \frac{1}{1 + sX} \tag{4.8}$$

where s is obtained from Eq.4.7 corrected for various experimental artifacts. A more rigorous approach consists in starting from the Bloch equations above and determining an approximate expression of many-body correlators as functions of two-body ones to obtain a closed set of equations [89]. This calculation is too complex to include dynamics or inhomogeneities, but gives qualitatively similar results.

4.3.3 Experiment

To measure an intensity-dependent phase shift of the intracavity probe beam, we used the scheme shown on Fig.4.2. We tuned the probe far from the $|g\rangle \rightarrow |e\rangle$ transition

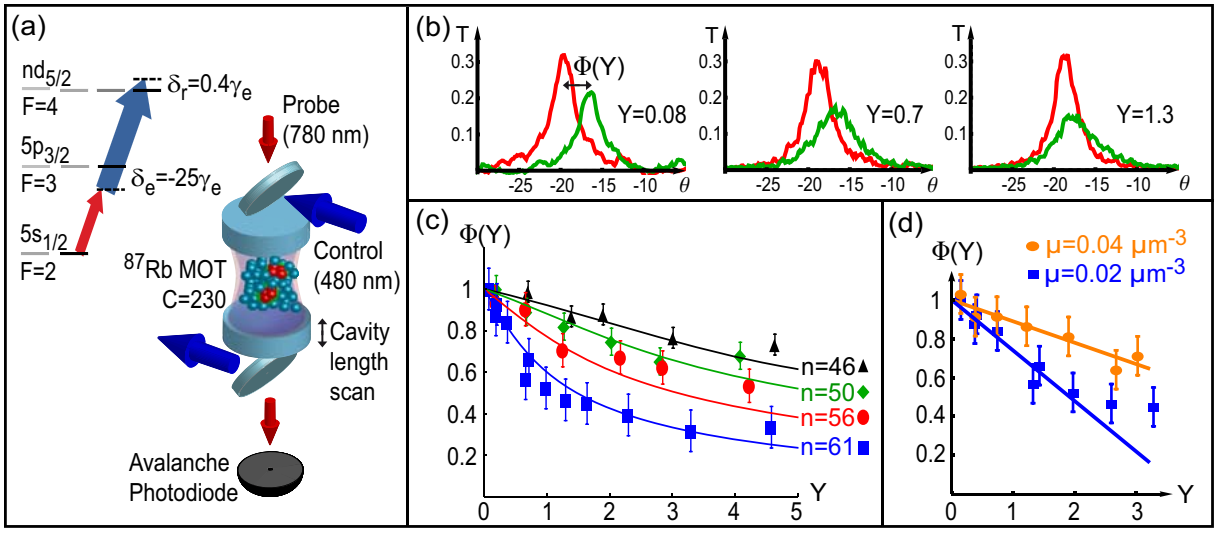

Figure 4.2: Measurement of an interaction-induced non-linear dispersion in a cold gaz (see text for details). (a) Atomic level scheme in ^{87}Rb used for off-resonant Rydberg state excitation, and experimental setup. A weak probe and a bright control beam are superimposed and injected into the cavity containing a cold gas of ^{87}Rb with a collective atom-light cooperativity $C = 230$. The cavity length is rapidly scanned to measure its resonance frequency ω_{res}. (b) Cavity resonance scans for increasing probe power Y, to determine the atomic polarisability α(($\theta = \omega_c/\gamma_c$, T is the cavity transmission normalized to that of a resonant empty cavity). Green curves are measured in presence of interactions (control beam on, Rydberg state $61d_{5/2}$), the red curves are used as a reference obtained for two-level atoms (control beam off) where $\alpha = \alpha_{2l}$. The normalized detuning Φ shifts from 1 to 0 as the interactions shift α from α_{3l} to α_{2l}. (c) $\Phi(Y)$ for Rydberg states $nd_{5/2}$ with different principal quantum numbers n and an atomic density $\mu = 0.04\ \mu m^{-3}$, interpolated without any free adjustment parameter by the blockade model including inhomogeneities and dynamics. (d) Dependence of the lowest-order χ^3 non-linearity on the density: decreasing the latter by a factor 2 decreases $\chi^3 \propto \mathrm{d}\Phi/\mathrm{d}t$ by ≈ 2 as well.

and measured the cloud's dispersion by scanning the length of the cavity and determining its resonance frequency ω_{res} from the probe's transmission. For a very weak probe we measured a "two-level" value ω_{2l} when the control beam was off, and a light-shifted "three-level" value ω_{3l} when the control beam off-resonantly coupled $|e\rangle$ to $|r\rangle$. We then progressively increased the impinging probe intensity Y, repeated this measurement, and determined the normalized resonance shift

$$\Phi(Y) = \frac{\omega_{res} - \omega_{2l}}{\omega_{3l} - \omega_{2l}} = \frac{\mathrm{Re}(\alpha - \alpha_{2l})}{\mathrm{Re}(\alpha_{3l} - \alpha_{2l})} \approx \frac{\alpha - \alpha_{2l}}{\alpha_{3l} - \alpha_{2l}}, \tag{4.9}$$

the approximation being valid in the far off-resonant regime. The second equality, easy to demonstrate, allows us to directly deduce α from $\Phi(Y)$ and compare it with the blockade model.

We observed that this shift $\Phi(Y)$ decreased from 1 towards 0 as expected from the blockade model: the higher the probe power, the more atoms were blockaded and effectively responded as two-level atoms. The quantitative agreement with this model was also satisfactory. In particular, in the low-intensity limit we verified that the $\chi^{(3)}$ non-linearity scaled as

$$\chi^{(3)} \propto \frac{\mathrm{d}\Phi}{\mathrm{d}Y}(0) = s = n_b \frac{\mathrm{d}\sigma_{33}}{\mathrm{d}Y}(0) \propto \mu V_b : \tag{4.10}$$

- We decreased the density μ by a factor 2 keeping all other parameters constant and checked that the resonance shift rate $\frac{\mathrm{d}\Phi}{\mathrm{d}Y}(0)$ decreased by the same amount, which clearly confirmed that the optical non-linearity was induced by interactions between different atoms rather than by single-atom effects.

- We varied the Rydberg state's principal quantum number n and checked that $\frac{\mathrm{d}\Phi}{\mathrm{d}Y}(0)$ scaled as $V_b \propto \sqrt{C_6} \propto n^{*11/2}$.

Nevertheless, the blockade model does not encapsulate all the physics involved in this process. In particular, it predicts that at high probe powers the average polarizability α should tend towards the value α_{2l} measured without control beam. While it is true for the real part of α governing the dispersion, the absorption remains stronger than expected due to additional dephasing mechanisms. This is not surprising given the simplicity of the blockade model, which ignores the fact that photons propagate through the cloud as delocalized polarisation waves. Interactions between these polaritons create inhomogeneous dephasings and act as a scattering mechanism, which can actually be turned to an advantage for creating single photons [79]. This type of effects will be discussed in more detail in Section 4.5.

4.3.4 Conclusion: strength of the non-linearity

Among all ways to quantify our system's non-linearity, I will chose a pragmatic, QIP-oriented one. Assuming that we drive the cavity with optical pulses and that the system returns to its ground state after each excitation, how many photons should these pulses contain to get a non-linear phase shift ~ 1 rad? In a continuous-wave picture, this translates into a number of photons per system's slowest decay time. If two photons are enough, there is good hope that this system can be used for photonic QIP.

In our case, a shift of the cavity resonance by one linewidth would shift the phase of the reflected probe beam by $\pi/2$. To obtain this resonance shift we need ≈ 3 nW

of optical power, which corresponds to $\sim 10^4$ photons per overall decay time limited to $\approx 1\ \mu s$ by the Rydberg excitation dynamics. Therefore, in this experiment we achieved a dispersive non-linearity comparable to the single-atom CQED case presented in the previous chapter, but not better. This was, however, the first experiment performed with this system, which left us quite some room for improvement as will be discussed in Section 4.5.

4.4 Homodyne tomography of a single photon retrieved from an atomic memory

For publications related to this section, see Appendix **??**,**??** *or Refs. [90, 91]*

4.4.1 Experimental protocol

Before pushing the interaction-induced non-linearities to the quantum limit, we decided to benchmark the "quantum optics" tools of our setup using a well-known protocol, and to determine whether a non-classical state prepared in our atomic gas could be efficiently transferred to a single-mode optical pulse. We used the well-established "DLCZ" scheme [92] to create a single collective atomic spin excitation and read it out as a single photon. This scheme had been implemented in a variety of configurations, in particular using cold atoms in cavities [93, 94]. However, besides demonstrating antibunching, these experiments provided little information about the prepared states' purity or modal structure. Moreover, although they could efficiently convert atomic excitations into intracavity photons, the probability to extract them in a single well-defined free-propagating mode remained limited.

In our experiment, sketched on Fig.4.3, we optically pumped the atoms in a ground state $|g\rangle$ and excited them with a very weak "write" laser pulse slightly detuned from an excited state $|e\rangle$. Once every ~ 1000 trials (~ 60 times per second), a cavity-stimulated hyperfine-state-changing Raman process occurred and an emitted "trigger" photon heralded the creation of a single delocalized atomic excitation in another ground state $|s\rangle$. The Raman process was then reversed: a bright "read" pulse coupled $|s\rangle$ to an excited state $|f\rangle$ with a detuning adjusted for the emitted "signal" Raman photon to be resonant with another cavity mode (3 free spectral ranges away from the trigger one). By aligning the beams to satisfy the phase-matching condition $\mathbf{k}_w + \mathbf{k}_r = \mathbf{k}_t + \mathbf{k}_s$ between the respective wavevectors of the write and read pulses and those of the trigger and signal photons, the atomic system returned to its initial state $|G\rangle = \prod_{j=1}^{N} |g\rangle_j$ with a near-unity efficiency while the signal photon was emitted from the cavity and directed either towards two photon counters in a Hanbury-Brown and Twiss configuration, or towards a balanced shot-noise-limited homodyne detector enabling a complete single-mode tomography of the emitted light state.

As I could witness in my previous projects, homodyne measurements can detect many things to which photon counters are blind, which makes them more insightful but also more challenging. For example, while the brightest possible "read" pulse provides the best photon's retrieval efficiency, it creates time-dependent light shifts inducing non-linear phase variations on the photon's field. This goes unnoticed in photon-counting measurements but decreases the interference visibility with the homodyne local oscillator. Our a-priori

calculations [91] showed that creating Fourier-transform-limited photons required smooth Gaussian-shaped laser pulses and carefully optimized experimental parameters.

4.4.2 Results

Time-resolved photon counting revealed that the trigger photon's temporal shape matched that of the write pulse as expected for a linear process. In contrast, the signal photon was emitted preferentially at the beginning of the read pulse as predicted by our theoretical calculations [91], and had a nearly-gaussian temporal profile $F(t) \approx \exp(-t^2/\tau^2)$ with a $\tau = 40$ ns duration. Photon correlation measurements confirmed that the "signal" photons were strongly antibunched.

When the signal photons were directed towards the homodyne detector, the bright continuous-wave local oscillator beam defined the measured spectral, spatial, and polarization modes. The temporal mode was selected by applying a Gaussian temporal filter $f(t) = \sqrt{F(t)}$ to the acquired homodyne signal $x(t)$, to obtain a single quadrature value $X = \int x(t)f(t)\mathrm{d}t$. From ≈ 100.000 such measurements we could reconstruct the full probability distribution $P(X)$ and apply a maximal-likelihood algorithm to determine the measured state, which showed 57% fidelity with a single photon and contain a negligible two-photon component. We could also include the homodyne detector's losses and noise in the reconstruction algorithm to determine state that we actually created. In this case the two-photon contribution remained low while the single-photon component increased to 82%, a record-high value given the fact that we did not compensate for losses occurring inside the vacuum chamber, considering them as intrinsic to our source. This $\eta = 82\%$ efficiency was quantitatively explained by a combination of several loss mechanisms, such as the spin-wave dephasing due to the finite atomic temperature, the finite cooperativity, the inhomogeneities of the laser beams, an imperfect optical pumping, or a mismatch between the trigger and signal intracavity standing waves.

Compared to similar experiments [93, 95], our system was not designed to obtain the best storage time for the spin wave but to maximize the photons's retrieval efficiency and to optimally control its mode. The cavity played an important role for this purpose. Besides enhancing the cooperativity, it defined the spatial and spectral modes of detected photons, which proved to be a crucial advantage compared to free-space experiments. At the same time, the input/output coupler was transmissive enough to be the main decay channel: once a photon was created inside the cavity, it could be recovered in the desired mode propagating outside the vacuum chamber with a $> 98\%$ probability. While both Raman-scattered photons were resonant with the cavity, the write and read laser pulses were off-resonant with it. This inhibited their Rayleigh scattering towards the photons counters, drastically decreasing "false positive" detection rates.

This experiment demonstrated our system's ability to manipulate and characterize light at the quantum level, which encouraged us to move forward and try to generate non-classical light states using Rydberg interactions.

4.5 Few-photon interactions in a Rydberg gas

For publications related to this section, see Appendix **??**,**??** *or Refs. [96, 97]*

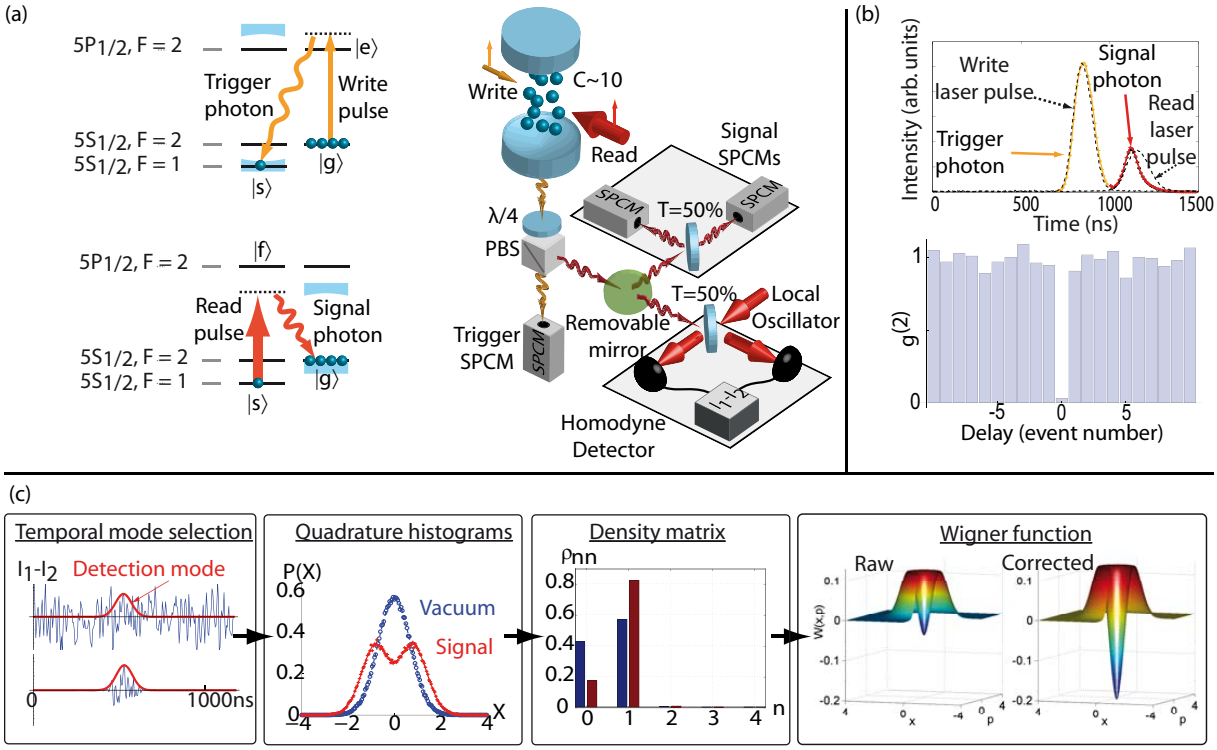

Figure 4.3: Homodyne tomography of single photons produced using the DLCZ protocol [92]. (a) Level scheme, and experimental setup. A cloud of N atoms is prepared in the state $|G\rangle = \prod_{j=1}^{N} |g\rangle_j$ ($|g\rangle = \left|5S_{1/2}, F = 2, m_F = 2\right\rangle$) and coupled to the cavity with a cooperativity $C \sim 10$. In presence of a weak "write" pulse, off-resonant with the state $|e\rangle = \left|5P_{1/2}, F = 2, m_F = 2\right\rangle$, a cavity-stimulated Raman process can create a single collective excitation in the state $|s\rangle = \left|5S_{1/2}, F = 1, m_F = 1\right\rangle$ heralded by a σ_+-polarized photon detected by the "trigger" photon counter (SPCM). The reverse process, driven by a bright "read" pulse detuned from the state $|f\rangle = \left|5P_{1/2}, F = 2, m_F = 1\right\rangle$, nearly deterministically returns the atomic system to its initial state and emits a σ_--polarized "signal" photon. After escaping the cavity, this photon is either split between two photon counters or analyzed by a balanced homodyne detector. (b) Time-resolved intensity measurements show that laser pulses and emitted photons have nearly Gaussian shapes consistent with theoretical predictions [91]. Correlations between events registered by the "signal" photon counters after a "trigger" event show that photons are strongly antibunched ($g^{(2)} = 0.04$ within the same pulse, $g^{(2)} \approx 1$ for different ones). (c) Homodyne tomography of the prepared state. The continuous homodyne signal is multiplied by a Gaussian filter determined from photon-counting measurements, and integrated to give a single value X of the phase-independent field's quadrature. The probability distribution $P(X)$, reconstructed from $\approx 100\,000$ quadrature measurements, shows a non-Gaussian shape, as opposed to the vacuum state measured as a reference. A maximal-likelihood algorithm is applied to $P(X)$ to reconstruct the state's diagonal density matrix with (right, red) or without (left, blue) correcting for imperfections of the homodyne detector. The corresponding Wigner functions both show negative values.

On the way towards deterministic photon-photon interactions, our next practical challenge was to enhance our system's non-linearity without creating strong losses. On the theoretical side, we had to account for quantum effects neglected in the classical version of the "blockade" model presented in Section 4.3.2.

4.5.1 Theoretical models

Blockade model

The simple model introduced in Section 4.3.2 predicts that atoms "blockaded" by a neighboring Rydberg atom are completely decoupled from the control beam, while atoms outside the blockade sphere feel no effect. This is of course a crude approximation which, among other things, neglects the fact that our Rydberg excitation process does not address specific atoms but creates collective excitations via the operator

$$\hat{J}^\dagger = \sum_{j=1}^{N} \hat{\sigma}_{rg}^{(j)} \tag{4.11}$$

In the interaction-less case, an optical coherent state $|\alpha\rangle \propto \exp(\alpha\hat{a}^\dagger)\,|0\rangle$ can then be transferred to the cloud as a coherent superposition of phase-matched polarisation waves $|\psi_\alpha\rangle \propto \exp(\alpha\hat{J}^\dagger)\,|G\rangle$ much like those discussed in the previous section.

When the intermediate state $|e\rangle$ is far off-resonant with light beams and can be adiabatically eliminated, one can transpose the blockade model to such delocalized polaritons by artificially dividing the cloud into $N_b = N/n_b$ "superatoms" and considering that the blockade mechanism allows each of these superatoms to contain at most one Rydberg excitation [98, 96]. The system is then formally equivalent to an ensemble of N_b non-interacting two-level atoms coupled to the cavity mode with a collectively-enhanced constant $g\sqrt{n_b}$. It can be described by an effective master equation involving the standard Tavis-Cummings hamiltonian

$$\hat{H}_{TC} = -\widetilde{\delta}_c \hat{a}^\dagger\hat{a} + \sum_{j=1}^{N_b} \left(-\widetilde{\delta}_r \hat{s}_j^\dagger \hat{s}_j + \widetilde{g}\sqrt{n_b}(\hat{a}^\dagger\hat{s}_j + \hat{a}\hat{s}_j^\dagger) \right) \tag{4.12}$$

where $\hat{s}_j$ annihilates the excitation of the j-th superatom and the effective parameters $\widetilde{\delta}_c$, $\widetilde{\delta}_r$ and $\widetilde{g}$ are obtained by adiabatically eliminating the intermediate atomic state $|e\rangle$ in the initial master equation (Eq.4.1a). This model preserves "delocalized" polaritons by replacing $\hat{J}^\dagger$ with $\hat{J}_s^\dagger = \sum_{j=1}^{N_b} \hat{s}_j$, creating a collective "super-atomic" excitation.

We used this model to calculate $g^{(2)}$ correlations of photons transmitted through a coherently-driven cavity containing an interacting off-resonant Rydberg gas [96]. Our practical motivation was to determine the range of experimental parameters where non-classical effects could be observed. We found that by increasing the cavity finesse by 10, reducing the mode waist to $15\mu m$ and loading the cloud in a dipole trap of a few $10\mu m$ in size, we should observe bunched or antibunched photon transmission depending on the cavity detuning. On resonance with the atom-shifted cavity, one injected photon prevents others from being transmitted (antibunching), whereas away from this resonance the opposite effect can lead to bunching. This experiment is planned for the near future.

Dephasing model

A major approximation of the blockade model is its "all or nothing" treatment of interactions. In reality, two atoms i and j in the cloud have a finite probability to be in the doubly-excited Rydberg state, which then acquires a time- and position-dependent phase shift $\phi = \kappa_{ij} t = C_6 t / R_{ij}^6$ due to interactions. Because atomic positions $\mathbf{r}_j$ are random, these pairwise phase shifts are random as well, and an initially phase-matched multiply-excited collective state becomes irreversibly dephased after a time $t_R \sim V^2/C_6$ where V is the excited volume. This mechanism was used in the experiment of Dudin and Kuzmich which demonstrated the first interaction-based single photon source [79, 99].

We used this "dephasing" model to study the evolution of a polaritonic state prepared in the cloud by exciting it with a very short classical pulse. When the number of created Rydberg excitations $|\alpha|^2$ is much smaller than the number of atoms, this initial state can be correctly approximated by a coherent polaritonic state

$$|\psi_{in}\rangle \approx \mathrm{e}^{-|\alpha|^2/2} \mathrm{e}^{\alpha \hat{J}^\dagger} |G\rangle \approx \mathrm{e}^{-|\alpha|^2/2} \sum_j \frac{\alpha^n}{\sqrt{n!}} |n\rangle , \tag{4.13}$$

$$|n\rangle = \frac{\hat{J}^n}{\sqrt{n!}} |G\rangle . \tag{4.14}$$

We consider that this state is left to evolve for a time t under the sole effect of interactions before being rapidly retrieved in the same optical mode as the excitation pulse. As interactions preserve the total number of Rydberg excitations, each n-excitation component evolves independently and only experiences an interaction-induced dephasing with respect to the initial phase-matched state $|n\rangle$:

$$|n(t)\rangle = \hat{U} |n\rangle = \exp\left(-i \sum_{j<k} \frac{C_6}{R_{ij}^6} \hat{\sigma}_{rr}^{(j)} \hat{\sigma}_{rr}^{(k)} \right) |n\rangle \tag{4.15}$$

The retrieval process, converting polaritons back to photons re-emitted in the excitation mode, can only access the fraction $\langle n| \hat{U} |n\rangle$ of this state that remains phase-matched with the initial state $|n\rangle$. We have shown in Ref.[97] that $\langle 2| \hat{U} |2\rangle$ has a relatively simple analytical expression and that for $n > 2$

$$\langle n| \hat{U} |n\rangle \approx \langle 2| \hat{U} |2\rangle^{n(n-1)/2} \tag{4.16}$$

The interaction-less terms $\langle 0| \hat{U} |0\rangle$ and $\langle 1| \hat{U} |1\rangle$ do not evolve while for $n > 1$ $\langle n| \hat{U} |n\rangle$ decreases and tends to 0 within a typical time $t_R \sim V^2/C_6$ consistent with the qualitative "dephasing" picture. In this simple model, the gas is expected to act as "quantum scissors" truncating an initially coherent state to leave only the zero- and one-photon components:

$$|\psi_{out}\rangle = \frac{|0\rangle + \alpha |1\rangle}{\sqrt{1 + |\alpha|^2}}. \tag{4.17}$$

This result needs again to be taken with caution, as decoherence mechanisms other that interaction-induced dephasing have been neglected.

4.5.2 Current direction: converting losses into phase shifts

While looking for a way to enhance our system's non-linearity, I realized that an important constraint, which we so far considered as unfortunate but unavoidable, was indeed relevant for most similar experiments but could be relaxed in our specific case.

In free-space experiments operating on resonance with atomic transitions, Rydberg interactions mainly lead to non-linear losses: non-linear dispersion can only be achieved by off-resonant excitation, which inevitably weakens the effect. But this no longer holds when atoms are placed inside a single-ended cavity, as shown on Fig.4.4:

- Assuming that the probe, resonantly driving the cavity mode, is also resonant with the $|g\rangle \rightarrow |e\rangle$ atomic transition and that the control beam resonantly couples $|e\rangle$ to $|r\rangle$ (i.e. $\delta_c = \delta_e = \delta_r = 0$), in absence of interactions the system is in the EIT condition. Provided that the round-trip linear losses L_0 in the atomic cloud are a few times smaller than the input/output coupler's transmission T, the probe enters the cavity and exits it with a phase shift $\phi = 0$. In classical terms, the cavity is said to be overcoupled.

- Now, if a single Rydberg atom creates losses L_1 a few times larger than T, the cavity becomes undercoupled: rather than being absorbed, the probe simply does not enter the cavity. It is directly reflected from the input/output coupler, but now with a phase $\phi = \pi$. A single photon injected in the cavity can then shift the phase of the following ones by π with little losses.

This idea is of course not new: in CQED experiments, it is the absorption created by one atom that modifies the cavity's transmission. Because this absorption is weak, cavity mirrors must have transmissions in the few ppm range and have therefore comparatively high scattering losses. In our case, it is not a single atom but a single "superatom" that creates the absorption. Because this superatom contains hundreds of atoms this absorption is much larger, and our $T = 5\%$ input/output transmission can already lead to such a "single-photon phase switching" effect for Rydberg states with $n \gtrsim 80$.

The regime $L_0 \ll T \ll L_1$ requires

- on one hand, a good EIT condition for single photons, i.e. a bright control beam uniformly illuminating all the atoms coupled to the cavity,

- on the other hand, a strong absorption per Rydberg blockade sphere, i.e. a large density and a high-lying Rydberg state.

Unfortunately, the transition dipole between the intermediate and the Rydberg states decreases as $n^{*-3/2}$, and in our initial experimental configuration the maximal control Rabi frequency Ω_c for $n \gtrsim 80$ was too low to reach a good EIT condition $L_0 \ll T$. To solve this problem we upgraded our experimental setup as shown on Fig. 4.5:

- After loading the MOT we confined the atoms in a red-detuned dipole trap formed by two orthogonal beams, one injected in the cavity and the other orthogonal to it. We optically depumped the atoms outside this trap to a dark state. The cavity mode was then coupled to a cloud with density $\mu \approx 0.06 \mu m^{-3}$ and a small characteristic size $\sim 30 \mu m$ which allowed us to focus the control beam more tightly and thus achieve a better EIT.

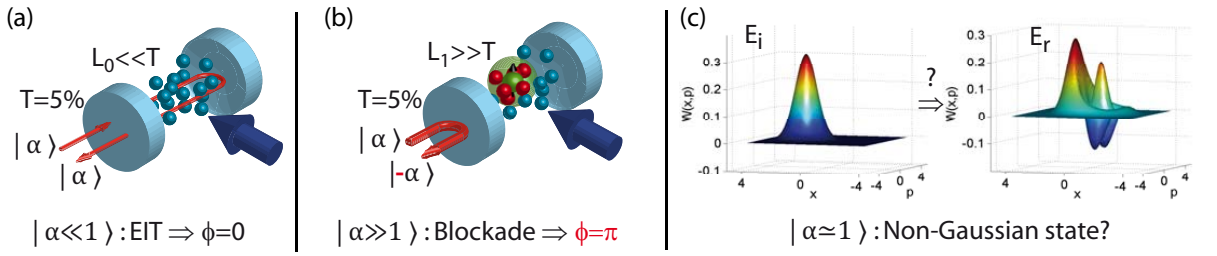

Figure 4.4: Transforming non-linear losses into non-linear phase shifts using a single-ended cavity. (a) The EIT condition provided by a bright Rydberg control beam allows a very weak coherent probe beam to resonantly couple in the cavity and exit it with a phase $\phi = 0$. This condition is satisfied when the double-pass losses L_0 in the cloud are much smaller than the input/output coupler's transmission T (= 5% in our case). (b) A single Rydberg atom excited by a bright coherent probe beam creates a blockade sphere, where the EIT condition is suppressed and atoms become strongly absorptive. If the double-pass losses L_1 exceed the transmission T, the probe beam becomes off-resonant. It is then reflected from the cavity with a phase $\phi = \pi$. (c) If the impinging field is in a coherent state $|\alpha = 1\rangle$ (left Wigner function) and the system shifts by π all but the zero- and one-photon components, the Wigner function of the reflected field (right) should become strongly non-Gaussian and negative.

- We added a confocal "buildup" Fabry-Perot cavity for the control beam, orthogonal to the "science" cavity already in place. The confocal configuration allowed the two counter-propagating intracavity beams to have different waists, reducing their interference and making the control Rabi frequency Ω_c reasonably uniform. This provided us with a power gain $G \approx 16$ and allowed us to reach sufficiently high Rydberg states while maintaining a good EIT at low probe power.

At the time of writing of this chapter, investigations along this line were still in progress. Theoretical models transposed to this resonant regime suggest that photon bunching or antibunching effects, depending on the cavity detuning, should be observed. Our first experimental observations are too preliminary to be presented here.

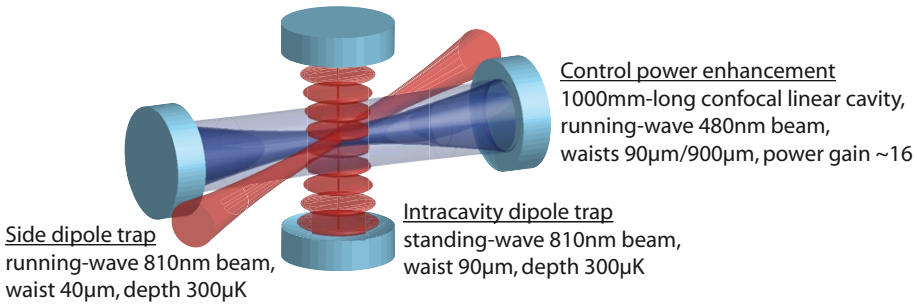

Figure 4.5: Upgrade of the experimental setup to observe interaction-induced non-linearities at the few-photon level. A system of two orthogonal dipole traps allows us to create a cloud with a $\mu \approx 0.06\mu m^{-3}$ density and a $\approx 30\mu m$ size (standard deviation of a Gaussian fit). A confocal buildup cavity for the Rydberg control beam provides a $G \sim 16$ power gain. The two beams counter-propagating inside this cavity have very different waists ($90\mu m$ for one, $90\mu m$ for the other), optimized to minimize the standing wave pattern and at the same time to create a beam wide enough to illuminate all trapped atoms in a relatively uniform way.

Chapter 5

Outlook and conclusion

Contents

5.1 On-going work **49**

5.2 Near-term projects **50**

5.3 General conclusion **50**

5.1 On-going work

The project on photon-photon interactions using Rydberg atoms presented in Chap.4 continues. Currently, we are observing our first "quantum" Rydberg-mediated effects, by measuring photon correlations in a probe beam transmitted through (or reflected from) the cavity containing the interacting atomic gas. Our immediate goal is to characterize all systematic effects in our experiment and to consistently interpret it with available theoretical models.

In a near future, we plan to fully characterize this deterministic non-classical light source by experimentally reconstructing the quantum state of a weak light pulse reflected from the cavity. Intuitively, if a single intracavity excitation switches its behavior from overcoupled to undercoupled, the impinging coherent laser pulse should experience a strong non-linear phase shift and be reflected in a non-Gaussian state which we could reconstruct by homodyne tomography (Fig. 4.4). Modeling this process quantitatively is another motivation for me to finish a theoretical work which I started nearly a year ago, with the aim of treating this system with minimal assumptions and reconciling the "blockade" and the "dephasing" models presented in Chap.4.

In parallel with our long-going theoretical collaboration with Étienne Brion from Laboratoire Aimé Cotton in Orsay, we also initiated a collaboration with the group of Anders Sørensen in Copenhagen to develop a realistic protocol for using this non-linear system as a logic gate acting on photonic qubits. A few theoretical problems need to be solved before experiments along this line can begin: find how to encode a "control' and a "target" qubit in this system, model the system's dynamics to optimize their temporal modes,...

5.2 Near-term projects

In January 2015 I will leave the Institut d'Optique and become an independent young team leader in the Physics Department of the Collège de France. My near-term plans are to keep investigating Rydberg-mediated photon-photon interactions, but to use several new ideas I had in the last few years. In particular, I would like to explore the fact that a Rydberg atom can influence ("blockade") a volume large enough to contain a gas with a periodic structure, which could lead to non-trivial interference effects enhancing the system's non-linearity. Overall, this physical system still has many possibilities to be explored, and many possible applications not only in QIP or in quantum optics but also in more fundamental studies of quantum physics. For instance, recent proposals suggest that interacting intracavity photons can behave as a two-dimensional fluid of massive charged particles, giving rise to interesting effects related to condensed-matter physics [4, 100].

5.3 General conclusion

In my research field, early-stage theorists often focus on a particular question, while experimentalists master a specific technique and look for questions it can answer. In this respect, as an experimentalist I chose an unusual, "theorist's" career path. My inborn love of practical knowledge made me learn many experimental methods, while my largely theoretical higher education helped me using them to investigate a particular problem in full depth. My competencies in this field are by no means exhaustive and, for example, my lack of expertise in condensed-matter techniques (especially nanofabrication) is patent, but at least to some extent I can now draw a panorama of what methods presented in this manuscript can do, and what's yet to be achieved.

Probabilistic projective measurements (Chap.2) are simple: non-linear crystals and linear optics, creating entangled resource states, don't need to be trapped, laser cooled, or optically pumped. Research efforts could then be focussed on other problems, which were solved before other approaches even faced them. As a result, this method still largely outperforms the others, but shows signs of saturation in terms of complexity authorized by "brute-force" experiments based on the standard "parametric crystals $\rightarrow$ linear optics $\rightarrow$ detectors" arrangement. Transposing them from bulk to integrated optics provides merely an illusion of scalability: one way or another, exponentially decreasing success rates need to be addressed.

Single atoms in cavities (Chap.3) are simple, but only on paper. Although this is rarely advertised in conference presentations, taking data on a CQED experiment may often resemble a shift on a particle accelerator, where sleepless nights follow each other for weeks. Claims like "this happens for technical reasons which we could fix in principle" become less audible with time, when it becomes clear that standard methods fail to work. Compared to bulk cavities, microresonators are a nice way of enhancing quality factors and moving towards more compact systems, but atoms get even more out of control due to van-der-Waals interactions with nearby surfaces. For these systems to become competitive for QIP, their overall duty cycles (fraction of time when an atom in the desired state is coupled to the cavity with the desired strength) must reach values at least comparable with success rates of projective measurements.

Large ensembles of correlated Rydberg atoms (Chap.4) are a theoretical conundrum.

Simple models, such as the "blockade" one, make rather intuitive and promising predictions, but their ability to reproduce experimental data comes almost as a surprise given how many things they neglect. Compared to other systems, Rydberg ensembles have many more degrees of freedom, and leaving some of them uncontrolled generally opens additional loss channels. In this respect, the idea of converting interaction-induced losses into phase shifts, presented at the end of the previous chapter, seems to be among the truly good ones I had so far: if the atomic cloud tends to become a lossy mess in presence of interactions, let's turn it to an advantage. Experimental results along this line are yet to come, but this is definitely a direction I will continue exploring.

These lines are written ten years after I started my PhD, five years after I launched our Rydberg-based project as a senior scientist, and two months before I move to Collège de France to create an independent team. Organizing my experimentalist's career in a "theorist's" fashion came at a cost: learning to operate complex experiments takes time, building them takes even longer. I disassembled and reassembled my PhD experiment twice, significantly upgraded the experiment in Munich, and built a lion's share of the Rydberg setup I'll leave behind in Institut d'Optique. As a result, I did not publish or collaborate as much as I could have, but I consider this choice as an investment: instead of my h-factor I improved my expertise.

Above all, during these years I learned how much the distinction between "fundamental" and "technical" problems is pointless. If an experiment disagrees with theory, refining the theory is as relevant as improving the experiment. It is my ability to do both which, professionally, got me out of tight corners. It is the possibility to do both which brought me into this field in the first place, and which makes me want to continue exploring it.

Bibliography

[1] R. Karplus and M. Neuman, Phys. Rev. **83**, 776 (1951).

[2] D. Bernard, F. Moulin, F. Amiranoff, A. Braun, J. Chambaret, G. Darpentigny, G. Grillon, S. Ranc, and F. Perrone, The European Physical Journal D - Atomic, Molecular, Optical and Plasma Physics **10**, 141 (2000).

[3] J. F. Corney, J. Heersink, R. Dong, V. Josse, P. D. Drummond, G. Leuchs, and U. L. Andersen, Phys. Rev. A **78**, 023831 (2008).

[4] I. Carusotto and C. Ciuti, Rev. Mod. Phys. **85**, 299 (2013).

[5] M. Wallquist, K. Hammerer, P. Rabl, M. Lukin, and P. Zoller, Physica Scripta **2009**, 014001 (2009).

[6] Z.-L. Xiang, S. Ashhab, J. Q. You, and F. Nori, Rev. Mod. Phys. **85**, 623 (2013).

[7] J. L. O'Brien, G. J. Pryde, A. G. White, T. C. Ralph, and D. Branning, Nature **426**, 264 (2003).

[8] A. Ourjoumtsev, Annales de Physique **32** (2008).

[9] R. Maiwald, A. Golla, M. Fischer, M. Bader, S. Heugel, B. Chalopin, M. Sondermann, and G. Leuchs, Phys. Rev. A **86**, 043431 (2012).

[10] M. K. Tey, Z. Chen, S. A. Aljunid, B. Chng, F. Huber, G. Maslennikov, and C. Kurtsiefer, Nature Physics **4**, 924 (2008).

[11] S. Haroche and J.-M. Raimond, *Exploring the Quantum: Atoms, Cavities, and Photons* (Oxford University Press, Oxford, 2006).

[12] Q. A. Turchette, C. J. Hood, W. Lange, H. Mabuchi, and H. J. Kimble, Phys. Rev. Lett. **75**, 4710 (1995).

[13] R. J. Schoelkopf and S. M. Girvin, Nature **451**, 664 (2008).

[14] J. P. Reithmaier, G. Sęk, A. Löffler, C. Hofmann, S. Kuhn, S. Reitzenstein, L. V. Keldysh, V. D. Kulakovskii, T. L. Reinecke, and A. Forchel, Nature **432**, 197 (2004).

[15] T. Yoshie, A. Scherer, J. Hendrickson, G. Khitrova, H. M. Gibbs, G. Rupper, C. Ell, O. B. Shchekin, and D. G. Deppe, Nature **432**, 200 (2004).

[16] R. Barends, J. Kelly, A. Megrant, A. Veitia, D. Sank, E. Jeffrey, T. C. White, J. Mutus, A. G. Fowler, B. Campbell, Y. Chen, Z. Chen, B. Chiaro, A. Dunsworth, C. Neill, P. O'Malley, P. Roushan, A. Vainsencher, J. Wenner, A. N. Korotkov, A. N. Cleland, and J. M. Martinis, Nature **508**, 500 (2014).

[17] V. Loo, C. Arnold, O. Gazzano, A. Lemaître, I. Sagnes, O. Krebs, P. Voisin, P. Senellart, and L. Lanco, Phys. Rev. Lett. **109**, 166806 (2012).

[18] M. D. Lukin and A. Imamoğlu, Phys. Rev. Lett. **84**, 1419 (2000).

[19] M. Bajcsy, S. Hofferberth, V. Balic, T. Peyronel, M. Hafezi, A. S. Zibrov, V. Vuletić, and M. D. Lukin, Phys. Rev. Lett. **102**, 203902 (2009).

[20] M. D. Lukin, M. Fleischhauer, R. Cote, L. M. Duan, D. Jaksch, J. I. Cirac, and P. Zoller, Phys. Rev. Lett. **87**, 037901 (2001).

[21] I. Friedler, D. Petrosyan, M. Fleischhauer, and G. Kurizki, Phys. Rev. A **72**, 043803 (2005).

[22] J. D. Pritchard, D. Maxwell, A. Gauguet, K. J. Weatherill, M. P. A. Jones, and C. S. Adams, Phys. Rev. Lett. **105**, 193603 (2010).

[23] A. Ourjoumtsev, R. Tualle-Brouri, J. Laurat, and P. Grangier, Science **312**, 83 (2006).

[24] A. Ourjoumtsev, R. Tualle-Brouri, and P. Grangier, Phys. Rev. Lett. **96**, 213601 (2006).

[25] A. Ourjoumtsev, H. Jeong, R. Tualle-Brouri, and P. Grangier, Nature **448**, 784 (2007).

[26] R. Tualle-Brouri, A. Ourjoumtsev, A. Dantan, P. Grangier, M. Wubs, and A. S. Sørensen, Phys. Rev. A **80**, 013806 (2009).

[27] J. Wenger, A. Ourjoumtsev, R. Tualle-Brouri, and P. Grangier, Eur. Phys. J. D **32**, 391 (2005).

[28] A. Dantan, J. Laurat, A. Ourjoumtsev, R. Tualle-Brouri, and P. Grangier, Opt. Express **15**, 8864 (2007).

[29] E. Schrödinger, Naturwissenschaften **23**, 807 (1935).

[30] M. Dakna, T. Anhut, T. Opatrný, L. Knöll, and D.-G. Welsch, Phys. Rev. A **55**, 3184 (1997).

[31] J. Wenger, R. Tualle-Brouri, and P. Grangier, Phys. Rev. Lett. **92**, 153601 (2004).

[32] N. Lee, H. Benichi, Y. Takeno, S. Takeda, J. Webb, E. Huntington, and A. Furusawa, Science **332**, 330 (2011).

[33] A. Ourjoumtsev, F. Ferreyrol, R. Tualle-Brouri, and P. Grangier, Nature Physics **5**, 189 (2009).

[34] A. Ourjoumtsev, A. Dantan, R. Tualle-Brouri, and P. Grangier, Phys. Rev. Lett. **98**, 030502 (2007).

[35] K. Wakui, H. Takahashi, A. Furusawa, and M. Sasaki, Opt. Express **15**, 3568 (2007).

[36] H. Takahashi, K. Wakui, S. Suzuki, M. Takeoka, K. Hayasaka, A. Furusawa, and M. Sasaki, Phys. Rev. Lett. **101**, 233605 (2008).

[37] X.-C. Yao, T.-X. Wang, P. Xu, H. Lu, G.-S. Pan, X.-H. Bao, C.-Z. Peng, C.-Y. Lu, Y.-A. Chen, and J.-W. Pan, Nature Photonics **6**, 225 (2012).

[38] P. R. Berman, ed., *Cavity quantum electrodynamics* (Advances in atomic, molecular, and optical physics, Academic Press, New York, 1994).

[39] R. J. Thompson, G. Rempe, and H. J. Kimble, Phys. Rev. Lett. **68**, 1132 (1992).

[40] A. Boca, R. Miller, K. M. Birnbaum, A. D. Boozer, J. McKeever, and H. J. Kimble, Phys. Rev. Lett. **93**, 233603 (2004).

[41] P. Maunz, T. Puppe, I. Schuster, N. Syassen, P. W. H. Pinkse, and G. Rempe, Phys. Rev. Lett. **94**, 033002 (2005).

[42] T. Aoki, B. Dayan, E. Wilcut, W. P. Bowen, A. S. Parkins, T. J. Kippenberg, K. J. Vahala, and H. J. Kimble, Nature **443**, 671 (2006).

[43] I. Schuster, A. Kubanek, A. Fuhrmanek, T. Puppe, P. W. H. Pinkse, K. Murr, and G. Rempe, Nature Phys. **4**, 382 (2008).

[44] T. Fischer, *Controlling the motion of an atom in an optical cavity*, Ph.D. thesis, Technische Universität München (2003).

[45] P. L. W. Maunz, *Cavity Cooling and Spectroscopy of a Bound Atom-cavity System*, Ph.D. thesis, Technische Universität München (2005).

[46] T. A. Puppe, *Trapping and observing single atoms in the dark*, Ph.D. thesis, Technische Universität München (2007).

[47] I. Schuster, *Nonlinear spectroscopy of a single-atom-cavity system*, Ph.D. thesis, Technische Universität München (2008).

[48] A. Kubanek, *Two-photon gateway and feedback control of a single atom in a cavity*, Ph.D. thesis, Technische Universität München (2010).

[49] M. Koch, *Classical and Quantum Dynamics of a Strongly Coupled Atom-Cavity System*, Ph.D. thesis, Technische Universität München (2011).

[50] A. Ourjoumtsev, A. Kubanek, M. Koch, C. Sames, P. W. Pinkse, G. Rempe, and K. Murr, Nature **474**, 623 (2011).

[51] A. Kubanek, A. Ourjoumtsev, I. Schuster, M. Koch, P. W. H. Pinkse, K. Murr, and G. Rempe, Phys. Rev. Lett. **101**, 203602 (2008).

[52] K. M. Birnbaum, A. Boca, R. Miller, A. D. Boozer, T. Northup, and H. J. Kimble, Nature **436**, 87 (2005).

[53] D. F. Walls and P. Zoller, Phys. Rev. Lett. **47**, 709 (1981).

[54] H. J. Carmichael, Phys. Rev. Lett. **55**, 2790 (1985).

[55] A. Lambrecht, T. Coudreau, A. M. Steinberg, and E. Giacobino, Europhys. Lett. **36**, 93 (1996).

[56] A. Kubanek, M. Koch, C. Sames, A. Ourjoumtsev, P. W. Pinkse, K. Murr, and G. Rempe, Nature **462**, 898 (2009).

[57] M. Koch, C. Sames, A. Kubanek, M. Apel, M. Balbach, A. Ourjoumtsev, P. W. H. Pinkse, and G. Rempe, Phys. Rev. Lett. **105**, 173003 (2010).

[58] A. Kubanek, M. Koch, C. Sames, A. Ourjoumtsev, T. Wilk, P. Pinkse, and G. Rempe, Applied Physics B **102**, 433 (2011).

[59] P. Horak, G. Hechenblaikner, K. M. Gheri, H. Stecher, and H. Ritsch, Phys. Rev. Lett. **79**, 4974 (1997).

[60] P. Maunz, T. Puppe, I. Schuster, N. Syassen, P. W. H. Pinkse, and G. Rempe, Nature **428**, 50 (2004).

[61] S. Nußmann, K. Murr, M. Hijlkema, B. Weber, A. Kuhn, and G. Rempe, Nature Physics **1**, 122 (2005).

[62] P. Bushev, D. Rotter, A. Wilson, F. m. c. Dubin, C. Becher, J. Eschner, R. Blatt, V. Steixner, P. Rabl, and P. Zoller, Phys. Rev. Lett. **96**, 043003 (2006).

[63] B. D'Urso, B. Odom, and G. Gabrielse, Phys. Rev. Lett. **90**, 043001 (2003).

[64] M. Koch, C. Sames, M. Balbach, H. Chibani, A. Kubanek, K. Murr, T. Wilk, and G. Rempe, Phys. Rev. Lett. **107**, 023601 (2011).

[65] R. Reimann, W. Alt, T. Kampschulte, T. Macha, L. Ratschbacher, N. Thau, S. Yoon, and D. Meschede, ArXiv e-prints (2014), arXiv:1408.5874 [quant-ph] .

[66] Y. Colombe, T. Steinmetz, G. Dubois, F. Linke, D. Hunger, and J. Reichel, Nature **450**, 272 (2007).

[67] D. O'Shea, C. Junge, J. Volz, and A. Rauschenbeutel, Phys. Rev. Lett. **111**, 193601 (2013).

[68] I. Shomroni, S. Rosenblum, Y. Lovsky, O. Bechler, G. Guendelman, and B. Dayan, Science **345**, 903 (2014), http://www.sciencemag.org/content/345/6199/903.full.pdf .

[69] T. G. Tiecke, J. D. Thompson, N. P. de Leon, L. R. Liu, V. Vuletić, and M. D. Lukin, Nature **508**, 241 (2014).

[70] I. Fushman, D. Englund, A. Faraon, N. Stoltz, P. Petroff, and J. Vučković, Science **320**, 769 (2008), http://www.sciencemag.org/content/320/5877/769.full.pdf .

[71] T. Volz, A. Reinhard, M. Winger, A. Badolato, K. J. Hennessy, E. L. Hu, and A. Imamoğlu, Nature Photonics **6**, 605 (2012).

[72] T. F. Gallagher, *Rydberg atoms* (Cambridge University Press, Cambridge, 1994).

[73] M. Saffman, T. G. Walker, and K. Mølmer, Rev. Mod. Phys. **82**, 2313 (2010).

[74] A. Osterwalder and F. Merkt, Phys. Rev. Lett. **82**, 1831 (1999).

[75] A. K. Mohapatra, M. G. Bason, B. Butscher, K. J. Weatherill, and C. S. Adams, Nature Physics **4**, 890 (2008).

[76] D. Jaksch, J. I. Cirac, P. Zoller, S. L. Rolston, R. Côté, and M. D. Lukin, Phys. Rev. Lett. **85**, 2208 (2000).

[77] J. D. Pritchard, K. J. Weatherill, and C. S. Adams, Non-linear optics using cold rydberg atoms, in *Annual Review of Cold Atoms and Molecules* (World Scientific, 2013) Chap. 8, pp. 301–350.

[78] A. K. Mohapatra, T. R. Jackson, and C. S. Adams, Phys. Rev. Lett. **98**, 113003 (2007).

[79] Y. O. Dudin and A. Kuzmich, Science **336**, 887 (2012).

[80] Y. O. Dudin, L. Li, F. Bariani, and A. Kuzmich, Nature Physics **8**, 790 (2012).

[81] Y. O. Dudin, F. Bariani, and A. Kuzmich, Phys. Rev. Lett. **109**, 133602 (2012).

[82] L. Li, Y. O. Dudin, and A. Kuzmich, Nature **498**, 466 (2013).

[83] T. Peyronel, O. Firstenberg, Q.-Y. Liang, S. Hofferberth, A. V. Gorshkov, T. Pohl, M. D. Lukin, and V. Vuletić, Nature **488**, 57 (2012).

[84] O. Firstenberg, T. Peyronel, Q.-Y. Liang, A. V. Gorshkov, M. D. Lukin, and V. Vuletić, Nature **502**, 71 (2013).

[85] C. S. Hofmann, G. Günter, H. Schempp, M. Robert-de Saint-Vincent, M. Gärttner, J. Evers, S. Whitlock, and M. Weidemüller, Phys. Rev. Lett. **110**, 203601 (2013).

[86] H. Gorniaczyk, C. Tresp, J. Schmidt, H. Fedder, and S. Hofferberth, Phys. Rev. Lett. **113**, 053601 (2014).

[87] Y. B. Ovchinnikov, Optics Communications **249**, 473 (2005).

[88] V. Parigi, E. Bimbard, J. Stanojevic, A. J. Hilliard, F. Nogrette, R. Tualle-Brouri, A. Ourjoumtsev, and P. Grangier, Phys. Rev. Lett. **109**, 233602 (2012).

[89] J. Stanojevic, V. Parigi, E. Bimbard, A. Ourjoumtsev, and P. Grangier, Phys. Rev. A **88**, 053845 (2013).

[90] E. Bimbard, R. Boddeda, N. Vitrant, A. Grankin, V. Parigi, J. Stanojevic, A. Ourjoumtsev, and P. Grangier, Phys. Rev. Lett. **112**, 033601 (2014).

[91] J. Stanojevic, V. Parigi, E. Bimbard, R. Tualle-Brouri, A. Ourjoumtsev, and P. Grangier, Phys. Rev. A **84**, 053830 (2011).

[92] L.-M. Duan, M. Lukin, J. I. Cirac, and P. Zoller, Nature **414**, 413 (2001).

[93] X.-H. Bao, A. Reingruber, P. Dietrich, J. Rui, A. Dück, T. Strassel, L. Li, N.-L. Liu, B. Zhao, and J.-W. Pan, Nature Physics **8**, 517 (2012).

[94] J. Simon, H. Tanji, J. K. Thompson, and V. Vuletić, Phys. Rev. Lett. **98**, 183601 (2007).

[95] A. G. Radnaev, Y. O. Dudin, R. Zhao, H. H. Jen, S. D. Jenkins, A. Kuzmich, and T. A. B. Kennedy, Nature Physics **6**, 894 (2010).

[96] A. Grankin, E. Brion, E. Bimbard, R. Boddeda, I. Usmani, A. Ourjoumtsev, and P. Grangier, New Journal of Physics **16**, 043020 (2014).

[97] J. Stanojevic, V. Parigi, E. Bimbard, A. Ourjoumtsev, P. Pillet, and P. Grangier, Phys. Rev. A **86**, 021403 (2012).

[98] C. Guerlin, E. Brion, T. Esslinger, and K. Mølmer, Phys. Rev. A **82**, 053832 (2010).

[99] F. Bariani, P. M. Goldbart, and T. A. B. Kennedy, Phys. Rev. A **86**, 041802 (2012).

[100] R. Umucalılar and I. Carusotto, Phys. Lett. A **377**, 2074 (2013).